UNIVERSIDAD POLITÉCNICA DE MADRID

ESCUELA TÉCNICA SUPERIOR DE INGENIERÍA AGRONÓMICA, ALIMENTARIA Y DE BIOSISTEMAS

MÁSTER EN BIOLOGÍA COMPUTACIONAL

CENTRO DE TECNOLOGÍA BIOMÉDICA (CTB) UPM

DEPARTAMENTO DE LENGUAJES Y SISTEMAS INFORMÁTICOS E INGENIERÍA DEL SOFTWARE

In silico repurposing approach to elucidate novel drug treatments for multiple sclerosis

MASTER FINAL THESIS

Author: Elizabeth Hyunjin Kwon

Professional tutor: Paloma Tejera Nevado

Academic tutor: Lucía Prieto Santamaria

July, 2025

Abstract

Multiple Sclerosis (MS) is a chronic, neurodegenerative disease marked by demyelination of neurons, the formation of plaques in the central nervous system, and progressive neurological disability. Although treatments exist for relapsing forms of MS, there remains a significant unmet need for therapies that can promote myelin regeneration, improve patient quality of life, and slow disease progression. This thesis investigates in silico drug repurposing as a strategy for identifying novel therapeutic candidates for MS, leveraging hypotheses generated by the DRIVE platform, a network-based medicine tool that integrates phenotypic, biological, and pharmacological data to suggest potential drug-disease relationships.

Two distinct pathways from DRIVE were examined: the gene-disease-drug pathway and the gene-protein-drug pathway, from which paclitaxel and isotretinoin were selected as candidate compounds. A multi-step filtering process, including Gene Ontology-based filtering, protein-protein interaction considerations, literature support, and structural availability, was used to prioritize the potential targets. Molecular docking was then conducted to evaluate the binding affinity of drug-target pairs.

Among the final candidates, docking analysis suggested that NLRP3 may serve as an alternative and therapeutically relevant target of paclitaxel in the context of MS. While these findings are preliminary and require further validation through molecular dynamics simulations and experimental studies, this work demonstrates the potential of combining network medicine approaches with structure-based drug repurposing tools to discover new therapies for diseases such as MS.

TABLE OF CONTENTS

Abbreviations

3D – Three Dimensional
AF – AlphaFold
AF3 – AlphaFold 3
API – Application Programming Interface
BBB – Blood-Brain Barrier
CNS – Central Nervous System
Cryo-EM – Cryo-Electron Microscopy
DAMPs – Damage-Associated Molecular Patterns
DMTs – Disease Modifying Therapies
DRIVE – Drug Repurposing In silico via Variable-pathway Exploration
dsDNA – double-stranded DNA
FDA – Food and Drug Administration
GO – Gene Ontology
HDN – Human Disease Network
HSDN – Human Symptoms Disease Network
IFN – Interferon
MMP – Matrix Metalloproteinase
MS – Multiple Sclerosis
NMR – Nuclear Magnetic Resonance
PAMPs – Pathogen-Associated Molecular Patterns
PDB – Protein Data Bank
pLDDT – predicted Local Distance Difference Test
PLIP – Protein–Ligand Interaction Profiler
PPI – Protein-Protein Interaction
PPMS – Primary Progressive Multiple Sclerosis
RMSD – Root Mean Square Deviation
RRMS – Relapsing Remitting Multiple Sclerosis
SPMS – Secondary Progressive Multiple Sclerosis

Index of Figures

Index of Tables

Section 1: Introduction and objectives

1.1 Multiple Sclerosis (MS): Background and the Current Treatment Landscape

Multiple Sclerosis (MS) is a chronic neurodegenerative disease of the central nervous system (CNS) that affects approximately 2.8 million people worldwide (1). It manifests in three main forms: Relapsing-remitting MS (RRMS), Primary Progressive (PPMS), and Secondary Progressive (SPMS), with RRMS being the most common (2).

MS is characterized by demyelination of neurons and axonal damage in the CNS, accompanied by plaque formation. This damage results from autoreactive immune cells crossing through the blood brain barrier (BBB), driven by impaired regulatory T cells and persistent activation of autoreactive, adaptive, and innate immune responses (3,4). There are several genetic and environmental risk factors that further affect disease severity (5).

Current treatments options for MS focus on reducing relapse rates and slowing MS progression (6,7), particularly applying to RRMS through disease-modifying therapies (DMTs) such as injectable interferon-β treatment (8) and glatiramer acetate (9). Meanwhile, the treatment options for PPMS and SPMS are limited, with ocrelizumab being the only Federal Drug Administration-approved drug to slow disease progression (10). Novel therapeutic targets that address progressive disease, promote neuroprotection, and repair existing damage are thus urgently needed.

1.2 Drug repurposing as a strategy to find new therapies

Classical drug development is costly and time-intensive, taking an average of 10-15 years and 2.5 billion dollars (11). Drug repurposing shortens this process significantly by identifying new uses for existing, approved treatments that already have established safety profiles (12).

Modern repurposing uses systematic approaches such as gene-expression based signature matching, pathway mapping, and clinical analysis to identify candidate drugs (13). These methods paired with virtual ligand screening, structure-based drug design, and docking, have further improved the efficacy of drug discovery.

In silico methods help prioritize candidates before they are validated experimentally. Molecular docking predicts binding affinity between drugs and target proteins (14), network pharmacology tools such as STRING database (15) or DRIVE (16) map drug effects on disease

pathways, and molecular dynamics simulations provide atom-level insights into binding stability and conformation (17).

1.3 Knowledge gap and thesis objectives

While network-based approaches like the ones present in DRIVE show promise for generating repurposing hypotheses in various diseases, their potential for identifying novel targets in MS remains unexplored. Furthermore, integrated pipelines combining hypothesis generation with in silico validation methods (e.g. docking, pathway analysis) for MS are limited.

This thesis aims to identify and validate drug-target predictions relevant to MS by using DISNET[1]-based disease-drug information and DRIVE[2]-based hypotheses, filtering methods, and molecular docking techniques. Secondary objectives include:

1. Developing a filtering pipeline to prioritize the most promising drug-target candidates for MS.
2. Evaluating top candidates with docking and reference binding site comparisons.
3. Justifying the therapeutic potential of final candidates based on computational and biological evidence.

The thesis is structured as follows: Section 2 discusses the state of the art of in silico drug repurposing tools; Then, Section 3 explains the methods used. Section 4 provides an overview of the results of the DRIVE prediction filtering pipeline and presents the docking results of the top hypotheses in comparison to previously described binding pockets of the selected drugs. In Section 5, these hypotheses are further discussed within the pathophysiological context, connecting them to previous MS drug research and their biological pathways. Finally, Section 6 notes the conclusions of this study and expands upon the current research for future directions.

[1] https://disnet.ctb.upm.es/
[2] https://live.drive-project.com/

Section 2: State of the Art of computational drug repurposing

2.1 Computational Drug Repurposing Tools

Drug repurposing applies in silico approaches to overcome traditional bottlenecks within drug discovery. Major strategies include signature mapping tools such as Connectivity Map, which matches gene expression signatures from diseases to discover new therapeutics (18); network pharmacology; molecular docking; and clinical data mining such as from electronic health records (19). This thesis focuses on a network-based hypothesis generation strategy, followed by structure-based molecular docking for validation.

2.2 Network medicine hypothesis generation

There are several strategies for identifying potential candidate targets. Pipelines using differential gene expression have been applied to diseases such as COVID-19 (20), as have proteomics-based approaches (21), and genome-wide position systems networks for patient-specific genetic profiles (22). Networks such as the Human Disease Network (HDN) (23) and the Human Symptoms-Disease Network (HSDN) (24), which connect diseases via genetic, biological, and protein interaction data, have also advanced drug discovery efforts. The DISNET expand upon these networks by extracting and consolidating information such as signs and symptoms from medical databases (e.g. Wikipedia and PubMed) and disease-gene associations from DisGeNET (25) to further improve drug repurposing strategies.

Leveraging information from DISNET, DRIVE generates novel disease-drug connections for diseases such as MS using various information paths (16). In this work, two information paths were used to find target candidates for certain drugs (**Figure 1**).

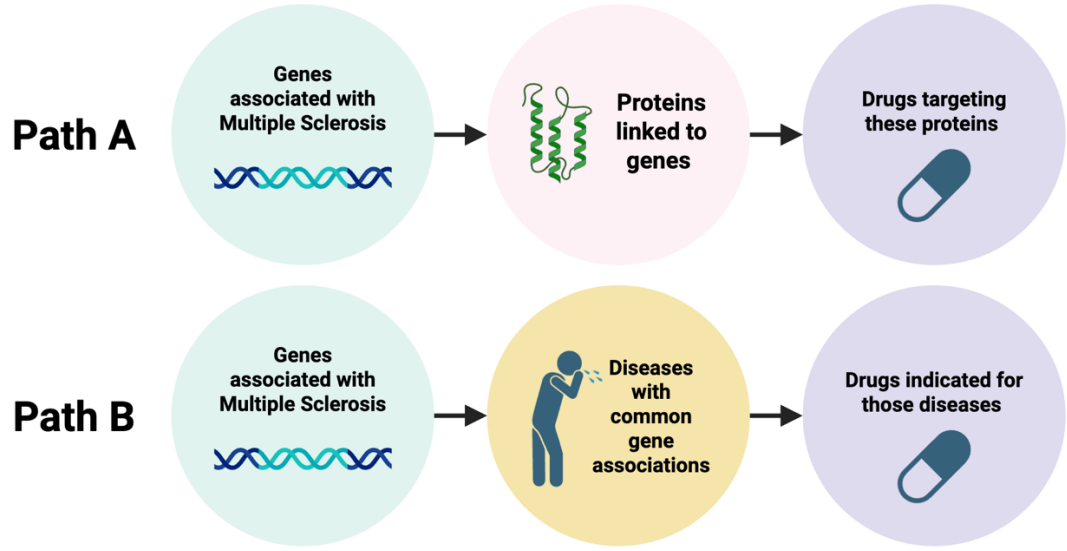

Figure 1. DRIVE-based information paths to generate drug-protein hypotheses
Created using BioRender and adapted from (16), Figure 1.

Path A takes the genes that are associated with the disease of interest, obtains diseases that share these gene associations and that are treated with the drug in question. Path B identifies the genes associated with the disease of interest, then finds proteins that are both associated with these genes and are considered targets of the drug of interest. While DRIVE suggests repurposing candidate hypotheses, further screening methods such as molecular docking are necessary to assess the feasibility of drug-target interaction before in-vitro or clinical validation.

2.3 Molecular Docking

Molecular docking predicts the geometry and binding affinity of a ligand to a three-dimensional (3D) protein target (14). By simulating the physical interactions between molecules, docking provides structural insight into potential drug-protein interactions. Docking has been used to help identify candidates like COVID-19 (26) and inhibitors for tuberculosis (27).

Structural accuracy of target proteins is critical for obtaining reliable docking predictions. While high-resolution experimental structures (derived from X-ray crystallography, NMR, or cryo-EM) are the preferred target inputs of docking software, AlphaFold 3 (AF3) has expanded docking possibilities (28). Still, AlphaFold-based docking should be carefully evaluated, as inaccuracies in binding site conformation may affect outcomes (29).

The typical docking workflow includes: **(1)** Binding site identification, **(2)** Ligand conformation sampling, and **(3)** Pose scoring based on energy functions (delta G, kcal/mol), incorporating van der Waals, hydrogen bonding, and electrostatic interactions.

Among available tools, AutoDock Vina is fast, accurate, and accessible, with benchmark studies showing 70-80% accuracy in reproducing experimental ligand poses (30). Other tools like GOLD (31) and Glide (32) also offer high accuracy and speed but often have steeper learning curves or license restrictions.

AutoDock Vina requires the preparation and input of a ligand and receptor, specification of a docking box (center and size), and configuration of various docking parameters (e.g. number of docking runs, scoring function, ligand flexibility). For less-characterized drug-target complexes, blind docking servers can dock without requiring previous knowledge of the binding site (14).

Template-based predict poses using structural analogs with known ligand conformations, leveraging similarities (33). While different docking programs define “similarity” distinctly, they typically use sequence identity (34), the threading (35), and structural alignments of the target proteins (36).

Web-based tools such as CB-Dock2 (37) and COACH-D (38) integrate both blind and template-based docking approaches. CB-Dock2, which employs AutoDock Vina as its main algorithm, has achieved 85.9% success in reproducing crystal structure poses. Given its accuracy and versatility, molecular docking is a valuable tool for prioritizing candidate targets. In this thesis, docking serves as the primary computational method for screening DISNET-derived drug-target pairs for further consideration.

Section 3: Materials and Methods

3.1 Data Origin: Target-drug hypotheses using DRIVE predictions and selection of drugs

Candidate drug-target hypotheses datasets were generated using the DRIVE dataset, which uses the DISNET database to infer possible drug-gene-disease associations. Two main information paths were used: Path A and Path B, summarized in **Figure 1.** From the DRIVE output, top drugs of interest were selected based on their results in these information paths and their redirection scores from the graph neural network (GNN) of the DRIVE methodology (39).

Six FDA-approved drugs (**Table S1**) emerged as potential MS treatments based on their association with MS-relevant genes via Path A, Path B, or both. Paclitaxel was selected for further analysis due to its strong redirection score and presence in both paths, strengthening the confidence of its relevance. A second drug, isotretinoin, was chosen for its comparatively lower toxicity.

To evaluate their novelty in MS treatment, both drugs were queried using the ClinicalTrials[3] Application Programming Interface (API) via the Python wrapper Pytrials. Code originally written by Esther Ugarte was modified[4] to automate retrieval of the number of registered clinical trials for each drug for MS. Neither paclitaxel nor isotretinoin had completed clinical trials related to MS in humans, supporting their novelty as repurposing candidates.

3.2 Selection of final target candidates for docking

Predicted gene targets were further refined through various filtering steps. The selection process differed slightly for each information path due to differences in the number and nature of the predictions. In Path A, limited DRIVE output led to a literature-driven expansion of candidates, whereas Path B required the reduction of the prediction sets through a series of filters. The following section outlines the approach taken for each path.

3.2.1 Selection of target candidates for Path A

For paclitaxel, there was only one candidate gene target for Path A. A literature search was performed on this one output, and alternative candidates were identified based on this search.

[3] https://clinicaltrials.gov/data-api/api
[4] https://medal.ctb.upm.es/internal/gitlab/disnet/in-silico-validation/tfm-elizabeth/blob/main/clinicaltrialsapi_code.py

3.2.2 Selection of target candidates for Path B

The initial DRIVE gene target prediction datasets for both isotretinoin and paclitaxel under Path B contained many entries. As manually performing docking and literature searches on the full outputs was not feasible, several preprocessing filters were applied using Python version 3.11.13. All code is available on GitHub[5], and the steps are outlined in **Figure 2.**

[5] https://medal.ctb.upm.es/internal/gitlab/disnet/in-silico-validation/tfm-elizabeth/tree/main/filtering_pipeline_code

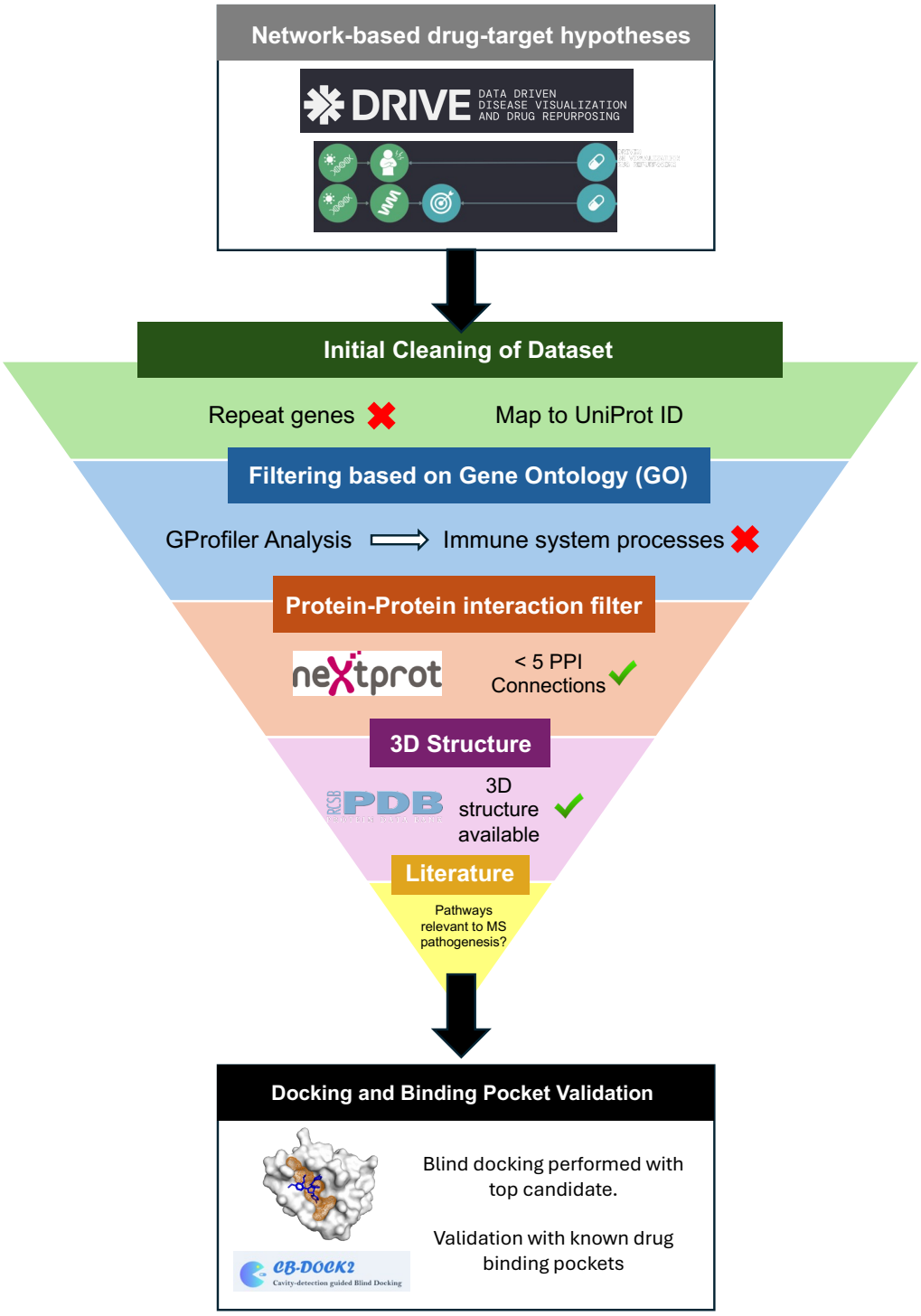

Figure 2. Visual summary of methodology and filtering steps

First, duplicate genes were removed. Then, a Gene Ontology (GO) statistical enrichment analysis was performed with the aid of the GProfiler package (version 1.0.0) on Python (40). Gene ID's of the filtered hypotheses were input into GProfiler, and an output of GO Biological Processes terms each with the list of intersecting genes was obtained. This work focused on identifying novel therapeutic targets, rather than prioritizing well-characterized immune genes. MS has a well-established immunopathological basis, and many immune-related genes, such

as those in the interleukin family, interferons, tumor necrosis factors, and chemokines, have already been studied extensively (41). Many of these, including cytokines such as interferon (IFN)-α, IFN-β, and IFN-γ, are not considered directly druggable by small molecules, limiting their relevance to docking. Thus, immune-associated genes enriched in Gene Ontology categories such as "immune system process" (GO:0002376) were excluded for both paclitaxel and isotretinoin. This allowed a more targeted exploration of lesser-studied biological pathways potentially relevant to MS.

Next, protein-protein interaction (PPI) data from neXTProt (September 2023 release) was used (42) to filter out *gene hubs*, genes with high connectivity in PPI networks. Genes with extensive interaction networks are often highly conserved and participate in fundamental cellular processes. Targeting such essential genes may increase the risk of off-target effects or toxicity, particularly if they are involved in multiple biological pathways, a rationale that aligns with the *centrality-lethality* rule, which suggests that highly connected proteins are more likely to be essential (43,44). To mitigate this risk, gene IDs from the target hypotheses were mapped to their corresponding UniProt IDs, and any proteins with more than five direct PPI connections in the neXtProt dataset were excluded from further analysis (45).

The remaining genes' UniProt IDs were used to check for available experimental 3D structures in the Protein Data Bank[6] (PDB). As docking was the primary screening tool in this thesis, the availability of even partial structures was important. Finally, literature reviews were conducted to determine which final targets had pathophysiological relevance to MS and had ligand-accessible structures.

3.3 Docking experiments

Molecular docking was performed on the final set of selected target candidates. The following section details the methodology used for these experiments, including query preparation, sources of input structures, use of AlphaFold models, consideration of domains, and binding pocket analysis.

3.3.1 Docking tools used

All docking was performed using CB-Dock2[7], an open-source server that uses the AutoDock Vina algorithm (37). Although CB-Dock2 automatically preprocesses submitted protein

[6] https://www.rcsb.org/
[7] https://cadd.labshare.cn/cb-dock2/index.php

structures, manual preprocessing was also applied (see *Section 3.3.2)* to improve accuracy, as supported by benchmarking studies demonstrating that manual preparation improved accuracy (46).

3.3.2 Preparation of proteins and ligands for docking

3D structures of top candidate targets were obtained from the PDB (**Table 1**). 3D ligand structures were acquired from PDB and PubChem[8]: Paclitaxel was isolated as a residue from PDB 1JFF using Chimera-X-1.19. Tretinoin was downloaded from PubChem (CID: 5282379). Although isotretinoin was initially selected based on DRIVE predictions, its lack of well-characterized targets relevant to its pharmacological action (47) made tretinoin (all-trans retinoic acid), an active metabolite of isotretinoin, more suitable for docking studies.

Table 1. Candidate target protein identifiers

Protein	UniProt ID	PDB Source
NLRP3	Q96P20	9MGY
MMP1	P03956	2CLT

Before docking was performed, candidate protein structures were preprocessed on Chimera-X-1.19. All ligands and residues (e.g. water molecules, ions, other small molecules) were removed from the protein structures, and hydrogen atoms and charges were added using the DockPrep tool. In cases where the target protein had essential ligand-coordinating ions, these ions were still omitted from the docking structure, as supported by evidence of previous benchmarks showing that their exclusion did not affect docking accuracy (46).

3.3.3 Generation and selection of AlphaFold models

In the case that a PDB structure had many incomplete regions from experimental methods, structural models were generated using AlphaFold Server[9] (powered by AlphaFold 3) to fill the gaps (28). To determine which of the five generated outputs was the best, each modeled structure was overlayed with the incomplete PDB structure with MatchMaker on Chimera-X-1.19. The calculated pruned Root Mean Square Deviation (RMSD) relative to the PDB structure, the sequency identity scores, and the overall predicted Local Distance Difference Test (pLDDT) scores were compared to select the best model.

[8] https://pubchem.ncbi.nlm.nih.gov/
[9] https://alphafoldserver.com/

3.3.4 Docking on targeted domains

For candidate proteins with large, multi-domain structures such as NLRP3, the focus was on a specific region of interest. Because docking tools generally perform with higher accuracy on focused or smaller regions (48), specific domains were isolated using ChimeraX. In the case of NLRP3, the NACHT domain (residues 133-679) was selected for docking. Although the core NACHT domain spans residues 220-536, a broader region was included to ensure structural context and stability during docking (**Figure 3**).

Figure 3. NLRP3 domain representation.
The PYD, NACHT, and LRR domain are labeled, with places where the NLRP3 proteins were cut indicated with dotted lines. Numbers correspond to the amino acid positions.

To compare resulting binding pockets from both the isolated domain and the full structure, MatchMaker was used. Overlapping pocket visualizations and binding residues were analyzed to verify that docking occurred on the same domain for both queries.

3.3.5 Generation of reference binding pockets for docking validation

For each drug of interest, a reference binding pocket was selected based on available crystallographic complexes and established direct binders. 3D complexes were analyzed using the Protein-Ligand Interaction Profiler[10] (PLIP) to identify interaction types with key binding residues (49) and inputted to CB-Dock2 to gather pocket information from template-based docking. Distances between paclitaxel and binding site residues were measured in ChimeraX. Data from PLIP and ChimeraX were used to generate a descriptive pocket illustration to serve as a reference for docking with candidate targets.

3.3.6 Analysis of docking experiment results

Docking results were analyzed by qualitatively comparing key binding site residues to those in the reference complexes (*Section 3.3.5*) for each drug. Key residues, cavity volumes, and Vina scores were obtained from the CB-Dock2 outputs. From the five docking results provided by CB-Dock2 for each protein-ligand pair, the "best" result was selected for further analysis based on combinations of lowest Vina score, similarity to the reference binding pocket, cavity

[10] https://plip-tool.biotec.tu-dresden.de/plip-web/plip/index

characteristics, and biological relevance (e.g. proximity to known functional domains or active sites).

Plausibility of binding was assessed qualitatively by evaluating key interactions, such as hydrogen bonds or hydrophobic contacts involving specific ligand functional groups, as well as distances to binding site residues and the Vina score. Visual inspection and analysis were performed using ChimeraX and PLIP to examine interaction types, measure residue-ligand distances, and generate pocket illustrations for comparison with reference complexes.

Section 4: Results

4.1 Overview of results of initial DRIVE outputs and clinical trials program

As described in the methodology, six FDA-approved drugs were identified from the DRIVE predictions as potential candidates for repurposing in MS. Among these, paclitaxel (labeled in **Figure S1**) and isotretinoin were selected for further investigation based on their DRIVE redirection scores and clinical considerations.

The DRIVE output datasets for each compound included target predictions from both Path A (genes-proteins-drugs) and Path B (genes-diseases-drugs):

- Path A yielded no candidate genes for isotretinoin, and one gene for paclitaxel.
- Path B yielded 1,632 and 6,661 candidate genes for isotretinoin and paclitaxel, respectively.

Candidate genes from both Path A and B were retained for downstream filtering and analysis.

4.2 Reference binding site reconstruction

To establish a structural baseline for evaluating docking results of top candidate targets, reference binding pockets were constructed for each drug using well-characterized targets with known direct interactions. For all isotretinoin-related docking experiments, its active metabolite tretinoin was used instead (see *Section 3.3.2)*. β-tubulin was chosen for paclitaxel (PDB: 1JFF) and CRABP1 for tretinoin (PDB: 1CBS). The reconstructed binding pockets, described below, provide a basis for later comparison with the binding sites predicted for candidate targets selected from the DRIVE hypotheses for paclitaxel and isotretinoin.

The binding pocket for paclitaxel is shown in **Figure 4** and **Table 2.** The pocket residues described by template-based docking include GLU22, VAL23, ASP26, GLU27, LEU217, ASP226, HIS229, LEU230, ALA233, SER236, GLY237, PHE272, PRO274, LEU275, THR276, SER277, ARG278, ARG320, PRO360, ARG369, GLY370, and LEU371. The cavity size was around 579 $Å^3$.

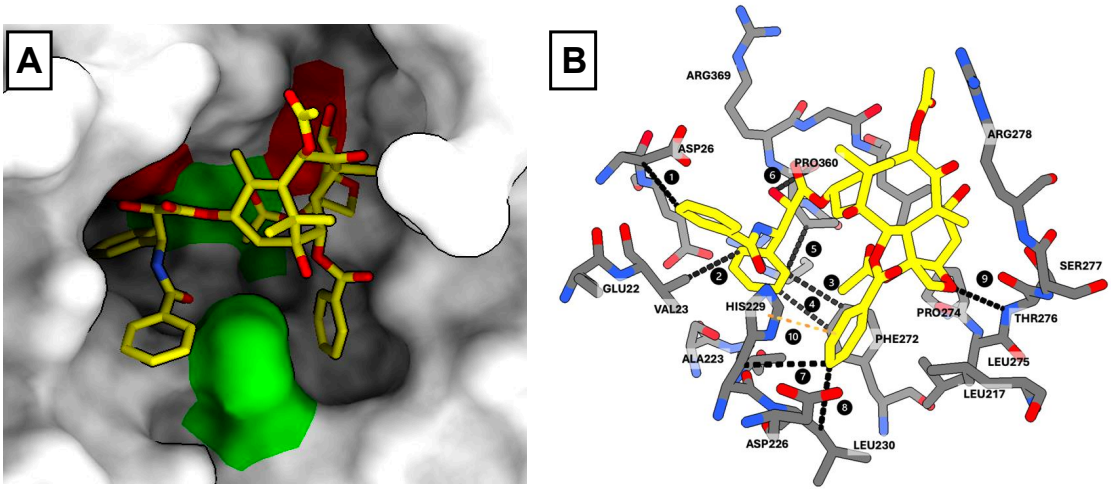

Figure 4. Paclitaxel binding site in β-tubulin.
A: Paclitaxel β-tubulin binding site. Green residues are aromatic and red are prolines. **B:** Key pocket residues are labeled. Interactions are shown in dotted lines, and the labeled numbers correspond with the annotations in **Table 2.**

Key pocket characteristics were: hydrogen bonding of the oxetane ring (interaction 9 on **Figure 4B)**; aromatic residues permitting π–π interactions with nearby rings of paclitaxel (interactions 10); presence of proline residues, one being near the polar interaction with oxetane ring; multiple hydrophobic interactions anchoring the C2, C3', and N' phenyl rings (interactions 1-5, 7, 8 on **Figure 4B**); and hydrogen bonding with the 2'-hydroxyl (interaction 6).

Table 2. Interaction annotations for paclitaxel-β-tubulin binding site
Interactions correspond with **Figure 4.**

Bond Number	Interaction type	Interacting Residue	Distance (Å)
1	Hydrophobic	ASP26	3.665
2	Hydrophobic	VAL23	3.490
3	Hydrophobic	PHE272	3.662
4	Hydrophobic	PHE272	3.404
5	Hydrophobic	PRO360	3.500
6	Hydrogen bonding	PRO360	3.508 (2.76 to H)
7	Hydrophobic	HIS229	3.925
8	Hydrophobic	LEU230	3.789
9	Hydrogen bonding	THR276	2.923 (2.30 to H)
10	Pi-stacking	HIS229	3.790

The binding pocket of tretinoin is visualized in **Figure 5** and **Table 3.** The pocket residues as described by template-based docking were PHE15, LEU19, VAL24, LEU28, ILE31, ALA32,

ALA35, ALA36, PRO39, THR54, THR56, VAL58, ARG59, VAL76, ASP77, ARG111, LEU121, MET123, ARG132, and TYR134. The cavity size was 1064 $Å^3$.

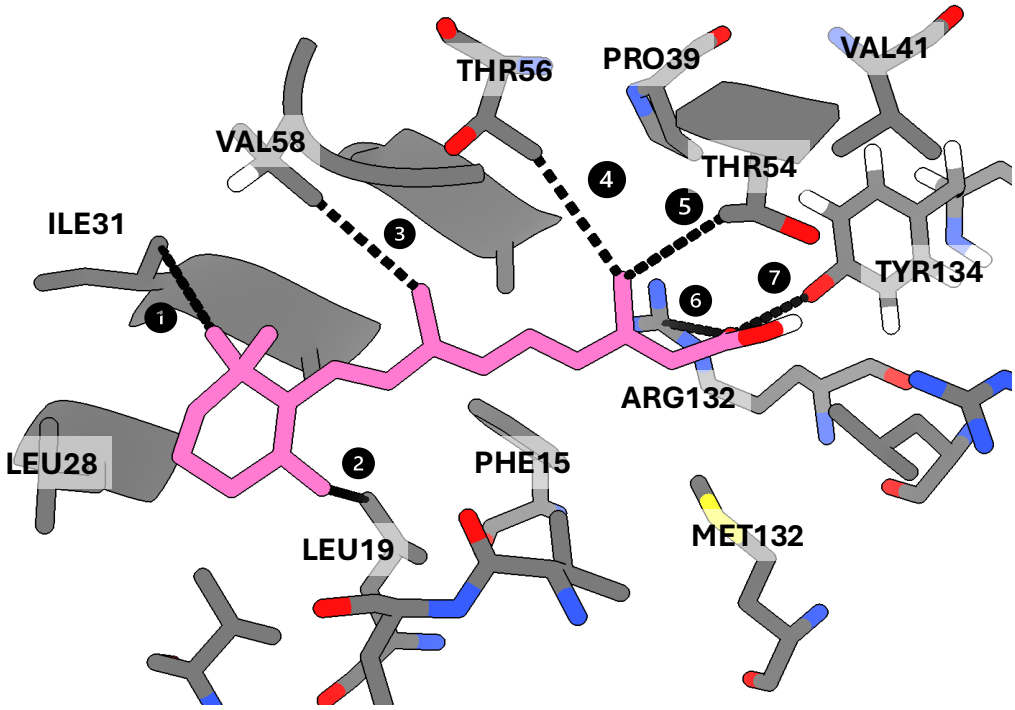

Figure 5. Tretinoin binding site in CRABPI
Key pocket residues are labeled. Interactions are shown in dotted lines, the adjacent numbers corresponding with the annotations in **Table 2.**

An essential salt bridge between ARG132 and the carboxylate group was annotated (interaction 6 in **Figure 5**). The pocket had several hydrophobic residues to stabilize the hydrocarbon tail of tretinoin, with ILE31, LEU19, VAL58, THR56, and THR54 (interactions 1-5), all with distances of maximum 4.096 Å (**Table 3**). Finally, there was one hydrogen bond interaction with TYR132, at 2.830 Å (interaction 7, **Table 3**).

Table 3. Interaction annotations for binding site interactions of tretinoin in CRABPI
Interactions correspond with **Figure 5.**

Interaction Number	Interaction type	Interacting Residue	Distance (Å)
1	Hydrophobic	ILE31	3.879
2	Hydrophobic	LEU19	3.992
3	Hydrophobic	VAL58	3.657
4	Hydrophobic	THR56	4.096
5	Hydrophobic	THR54	3.845
6	Salt Bridge	ARG132	3.480
7	Hydrogen bonding	TYR134	2.830

4.3 Path A: Repurposing candidate from the genes-proteins-drugs pathway predictions

Path A analysis yielded a single gene for paclitaxel, *BCL2*, and no outputs for isotretinoin. A manual literature review confirmed that a direct molecular interaction between BCL-2 protein and paclitaxel occurred. In addition, pathway analyses (discussed further in Discussion) identified NLRP3 (Uniprot: Q96P20) as a candidate target of interest. In this section, the docking results of NLRP3 with paclitaxel are described.

Docking was performed on the NACHT domain of NLRP3 due to its biological relevance. To ensure that the identified binding site was not an artifact of isolating the NACHT domain, the full structure was also docked with paclitaxel. The top-scoring binding pockets appeared in the same region on the NACHT domain in both cases (**Figure S2)**.

4.3.1 AF modeling of NLRP3

Because NLRP3 had several missing regions in the cryo-EM structure (PDB:9MGY), a structural model of the full-length human NLRP3 was generated with AF3. The best model had a mean pLDDT of 77.51, an RMSD of 0.893 Å to the cryo-EM structure, and a sequence identity score of 4376.6 out of 5000 (**Table S2**).

Docking simulations were conducted using the NACHT domain from both the cryo-EM structure of *NLRP3* (PDB:9MGY) and the AlphaFold-predicted model. In both cases, the same general binding region was identified, with some discrepancies in the binding conformation and positioning of the ligand (**Figure 6C**).

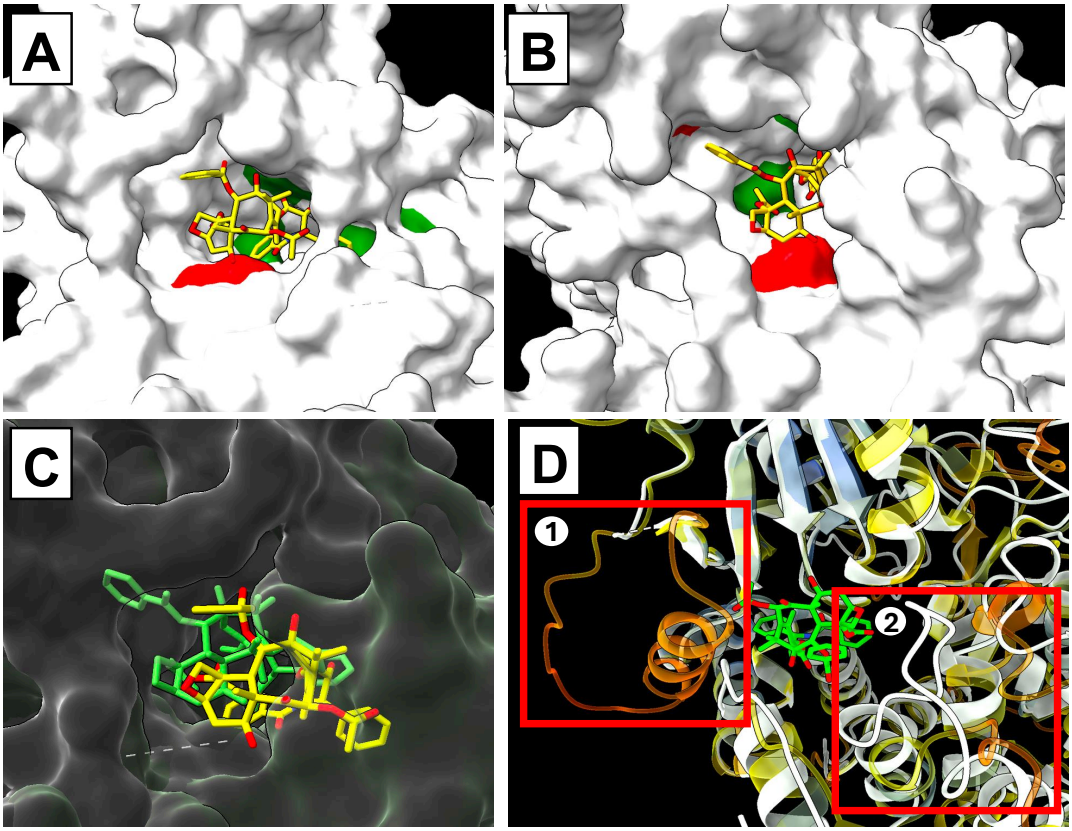

Figure 6. Comparison of docking sites of paclitaxel for cryo-EM and AlphaFold-generated NLRP3

A: predicted docking site of paclitaxel on the cryo-EM structure of NLRP3 NACHT domain (PDB: 9MGY). Green – aromatic residues; red – prolines. **B:** the predicted docking site of paclitaxel on the best AlphaFold-generated model of NLRP3. **C:** the binding conformations of the two queries overlapped using ChimeraX Matchmaker tool. Yellow – paclitaxel with AF model; Green – paclitaxel with cryo-EM model. **D:** AF-generated (multi-color) and cryo-EM (white) models' binding pockets overlapped. The red boxes mark the discrepancies between the two chains near the docking region (Box 1 – GLU176-SER201; Box 2 – LYS615-LEU628). The orange color of Box 1 indicates a pLDDT of between 50 and 70.

For both structures, the predicted pocket volume, docking score, and interacting residues are summarized in **Table 4.** The binding pockets of the two structures shared approximately 51.7% sequence identity relative to the cryo-EM structure. A key difference was the presence of residues GLN180, ARG183, GLU184, and LEU187 in the AF-predicted pocket, which aligned with a missing region (GLU176-SER201) in the cryo-EM model (**Figure 6D**). This predicted region on the AF-predicted structure had an orange color (left red box on **Figure 6D**), indicating moderate pLDDT. Given the greater completeness of the AF-generated structure pocket, it was retained for further analysis and validation with the reference pocket.

Table 4. Predicted docking of paclitaxel on NLRP3 NACHT region on the cryo-EM and AlphaFold-generated structures

Structure	Cavity Volume (Å³)	Vina Score (kcal/mol)	Predicted Pocket Residues
Cryo-EM NACHT	2526	-9.3	GLU176 GLN225 GLY226 ALA227 ALA228 ILE230 ARG351 PRO352 VAL353 LEU355 GLU369 ILE370 LEU371 GLY372 PHE410 ILE574 PHE575 ARG578 LYS620 GLN624 SER626 LEU628 TYR632 ASN656 LEU657 SER658 THR659 MET661 ASP662
AlphaFold NACHT	1855	-9.9	GLN180 ARG183 GLU184 LEU187 ALA227 ALA228 PRO352 VAL353 GLU356 PHE410 ILE411 THR439 THR524 GLY566 ILE574 PHE575 ARG578 PRO625 SER626 LEU628 GLU629 TYR632 SER658 THR659 MET661 ASP662

4.3.2 Residue interactions of Paclitaxel-NLRP3

In the AlphaFold-predicted NACHT domain, paclitaxel formed multiple interactions with the surrounding residues (**Figure 7, Table 5)**. All final interaction distances were under 4 Å. The binding pocket had a cavity of 1855 $Å^3$ and a Vina score of -9.9. Binding pocket residues are listed in **Table 4.**

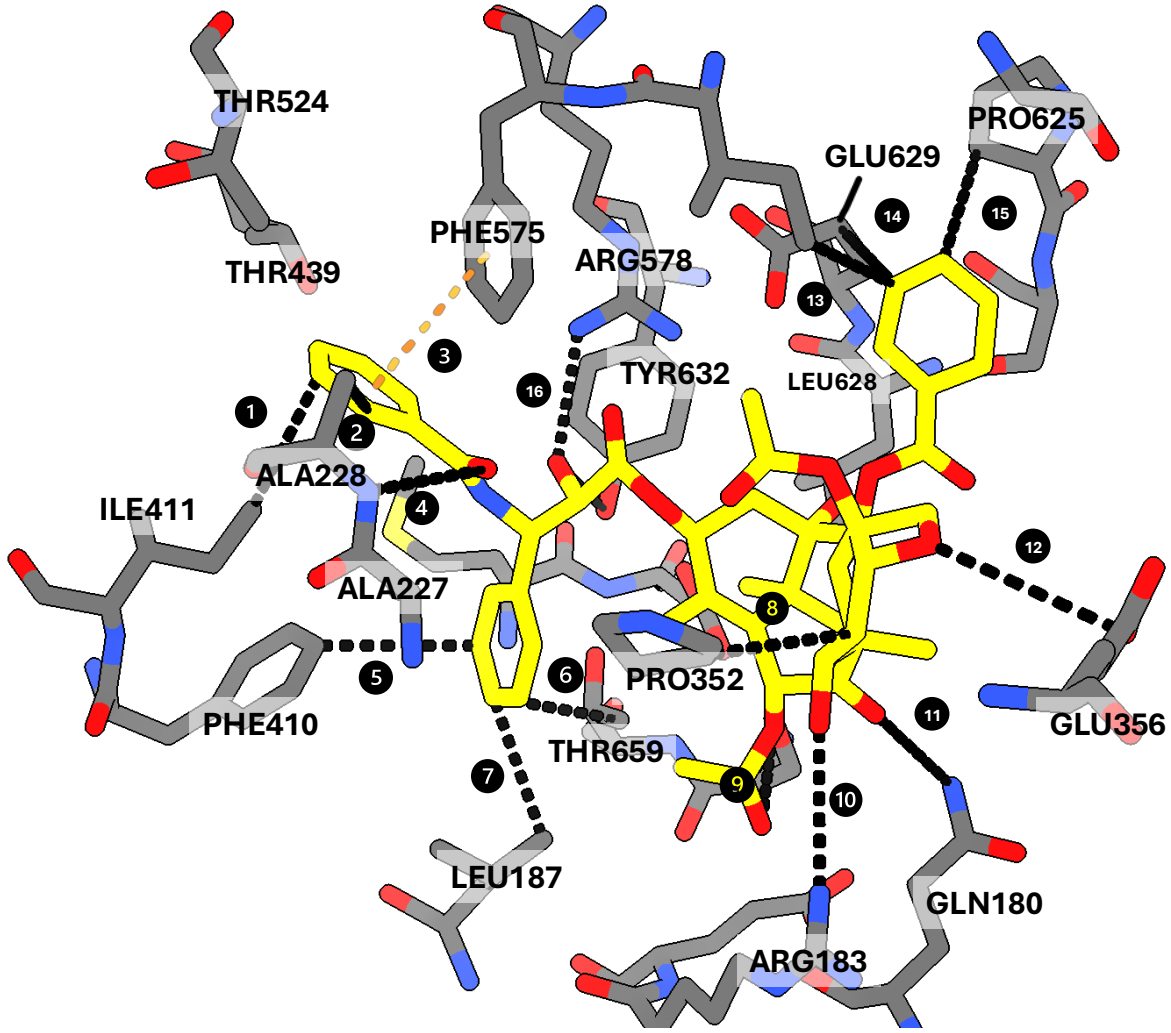

Figure 7. Predicted binding conformation of paclitaxel in NLRP3.
Key residues and proximal residues are labeled. Interactions are shown in dotted lines, and the labeled numbers correspond with the annotations in **Table 5.**

Notable interactions included: a hydrogen bond with the C2' side chain oxygen (interaction 4, **Table 5**) at 4.040 Å; a π–π interaction between the N' phenyl ring and PHE575 at 4.810 Å (interaction 3); and multiple hydrophobic interactions anchoring the C2 and C3' phenyl rings (interactions 1, 2, 5, 6, 13-15) with a maximum 3.990 Å. All interactions were identified by PLIP, except interaction 12 between the oxetane ring SER658 (**Table 5**), which was included due to its relevance in the reference paclitaxel binding pocket (interaction 9 of **Table 2**). Notably, the oxetane hydrogen bond distance was considerably longer in the NLRP3-NACHT pocket (4.927 Å) compared to the reference pocket (2.930 Å, **Table 2**). Other key characteristics of the pocket were aromatic residues (PHE410, PHE575) near paclitaxel's phenyl rings and general hydrophobicity, with eleven aliphatic residues (**Table 4**).

Table 5. Interaction annotations for predicted binding conformation of paclitaxel in AF model of NLRP3

Interactions correspond with **Figure 7.** * was not identified by PLIP.

Bond Number	Interaction type	Interacting Residue	Distance (Å)
1	Hydrophobic	ILE411	3.990
2	Hydrophobic	ALA228	3.872
3	π–π	PHE575	4.810
4	Hydrogen Bond	ALA228	4.040 (3.17 to H)
5	Hydrophobic	PHE410	3.937
6	Hydrophobic	THR659	3.497
7	Hydrophobic	LEU187	3.580
8	Hydrophobic	PRO352	3.605
9	Hydrogen bonding	SER658	3.819 (3.39 to H)
10	Hydrogen bonding	ARG578	3.685 (2.25 to H)
11	Hydrogen bonding	GLN180	3.207(2.87 to H)
12	Hydrogen bonding	SER658	4.927*
13	Hydrophobic	ILE574	3.420
14	Hydrophobic	GLU629	3.594
15	Hydrophobic	PRO625	3.938
16	Hydrogen bonding	GLN180	3.211 (2.87 to H)

The paclitaxel binding conformer varied from the β-tubulin-bound form, having rotations at carbons C3', C13, C2, and C10 atoms (**Figure 8**). The β-tubulin-bound paclitaxel (**Figure 8A)** adopted a more "closed" conformation, with the N' phenyl ring and C2 ring positioned closer to one another than in the NLRP3-docked conformer **(Figure 8B)**.

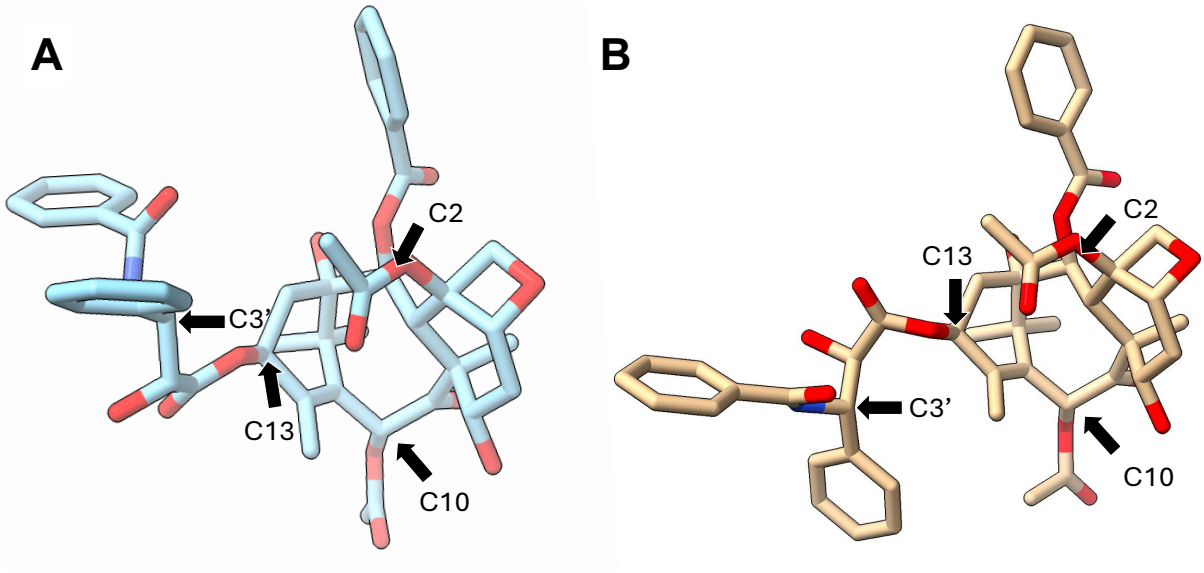

Figure 8. Comparison of paclitaxel binding conformers for docking with NLRP3.
A. Paclitaxel bound to β-tubulin (PDB:1JFF). **B:** Predicted binding conformation of paclitaxel in AlphaFold-generated *NLRP3* NACHT domain. Black arrows mark the carbon atoms around which torsional rotations occurred, resulting in conformational differences between **A** and **B**.

4.4 Path B: Repurposing candidate from the genes-diseases-drugs pathway predictions

In parallel with the literature-based target hypothesis from *Path A*, a systematic filtering was applied to prioritize drug-target candidates identified via Path B. From initial target gene lists of approximately 1,632 for isotretinoin and 6,661 for paclitaxel, 11 and 10 drug-target pairs, respectively, were retained for further analysis (**Tables S3 and S4**).

Among these candidates, *MMP1* (matrix metalloproteinase-1) appeared as a final candidate for both drugs and was of particular interest due to its biological relevance in MS and the availability of a high-resolution crystal structure suitable for docking.

Docking was performed using the crystal structure of MMP1 protein (PDB: 2CLT) for both compounds, the top two docking poses according to Vina scores are detailed in **Table S5 and 6.** Although the top-ranked binding site did not correspond to the catalytic region of MMP1, the second-ranked pocket did for both drugs. Given the functional importance of this region, docking poses with the second-best Vina scores were selected for further analysis.

4.4.1 Paclitaxel docked to MMP1

Paclitaxel was docked into a surface-exposed cavity adjacent to the catalytic zinc ion which coordinated with HIS199, HIS203, and HIS209. The Vina score of the binding conformation was -8.0, with a cavity volume of 228 $Å^3$. The contact residues identified can be found on

Table S5 under Pocket #2. Several key interactions were observed (**Figure 9, Table 6**), including hydrophobic interactions near the N' phenyl ring (interaction 1), potential weak coordination of the 2'-OH with the zinc atom (interaction 4), and hydrogen bonding with the oxetane ring (interaction 5).

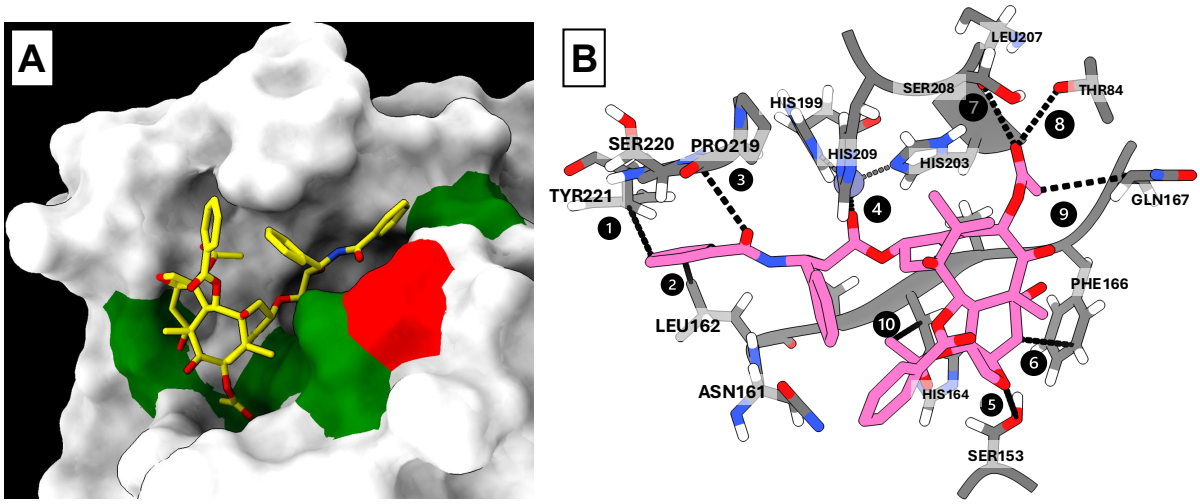

Figure 9. Binding pocket of paclitaxel docked to MMP1
A: Binding cavity of paclitaxel docked to MMP1. Green residues are aromatic and red are prolines. **B:** Key pocket residues are labeled. Interactions are visualized with dotted lines, with adjacent numbers corresponding to the annotations in **Table 6.**

The C3' phenyl ring and C2 ring did not have any hydrophobic interactions anchoring them to the pocket. There was one proline residue present in the identified binding pocket which participated in a hydrogen bond (interaction 3). All interactions were identified by PLIP, except interaction 4, which represents a potential zinc coordination at 1.391 Å. Hydrogen bonds were observed at 3.480, 3.019, and 3.079 Å (interaction 3, 7, 8, **Table 6**).

Table 6. Interaction annotations of MMP1-Paclitaxel binding pocket
The interaction number corresponds to the labels in **Figure 9B.** * not identified by PLIP.

Interaction Number	Interaction type	Interacting Residue	Distance (Å)
1	Hydrophobic	TYR221	3.758
2	Hydrophobic	LEU162	3.517
3	Hydrogen bonding	PRO219	3.480 (2.84 to H)
4	Zinc coordination	Zn^{2+}	1.391*
5	Hydrogen bonding	SER153	3.154
6	Hydrophobic	PHE166	3.792
7	Hydrogen bonding	LEU207	3.019 (2.67 to H)
8	Hydrogen bonding	THR84	3.079 (2.12 to H)
9	Hydrophobic	GLN167	3.914
10	Hydrophobic	HIS164	3.265

Compared to the β-tubulin-bound form, the docked paclitaxel conformer on MMP1 had rotations at carbons C13, C10, and C4, with C2' (**Figure 10**). However, both β-tubulin and MMP1-bound conformers maintained a similar conformation, with relative proximity between the phenyl groups.

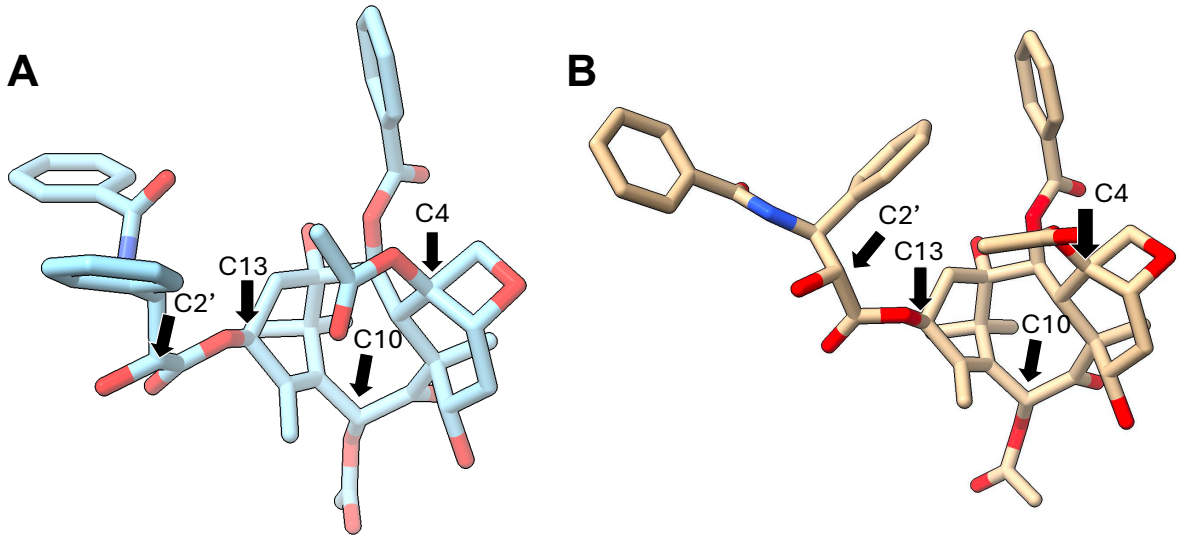

Figure 10. Comparison of paclitaxel binding conformers for docking with MMP1
A: Paclitaxel bound to β-tubulin (PDB:1JFF). **B:** Predicted paclitaxel conformation in MMP1. Black arrows mark the carbon atoms where rotations occurred.

4.4.2 Tretinoin docked to MMP1

Following the paclitaxel analysis, tretinoin was also docked to MMP1. The resulting binding pocket, located in the catalytic site near HIS199, HIS203, and HIS209, corresponded to the second highest vina score of -6.9, with a cavity volume of 228 $Å^3$. Contact residues can be found in **Table S6** under Pocket #2. Key interactions with the binding pocket included: hydrophobic interactions across the ligand structure (interactions 1-4 on **Figure 11, Table 7**) and hydrogen bonds with the carboxylate group of tretinoin (interactions 5 and 6). No salt bridge was observed between the carboxylate group and the pocket.

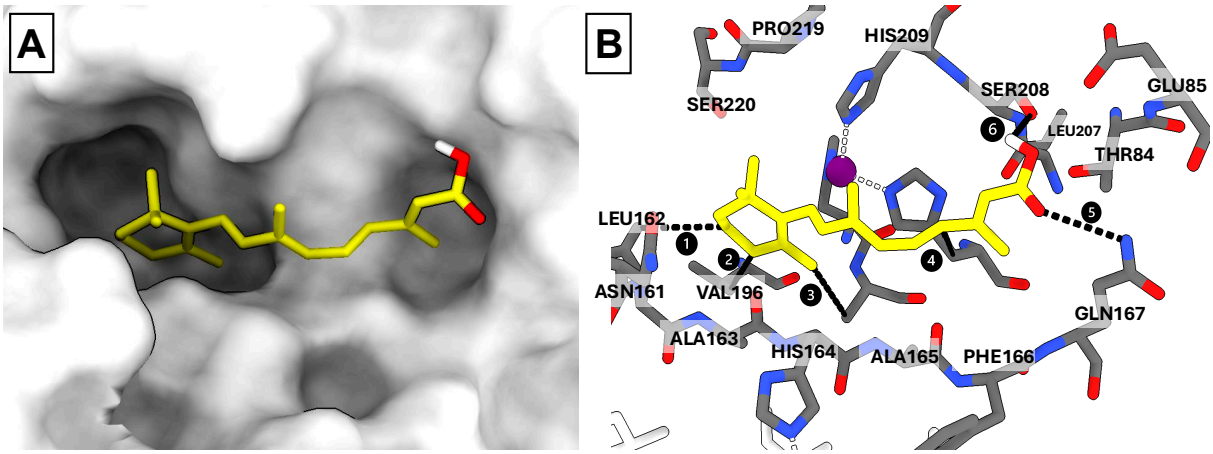

Figure 11. Binding pocket of tretinoin docked to MMP1
A: Binding cavity. **B:** Key pocket residues are labeled. The purple sphere is the Zn^{2+} ion. Interactions are visualized with dotted lines, with adjacent numbers corresponding to the annotations in **Table 7.**

No likely coordination was observed between the Zn^{2+} ion and tretinoin. Although a nearby methyl group was positioned close to the ion, it lacks a coordinating functional group and was thus excluded from the annotations. All annotated interactions within the binding pocket were within 3.979 Å of the ligand (**Table 7**).

Table 7. Distance calculations of MMP1-Tretinoin binding pocket.

Bond Number	Interaction type	Interacting Residue	Distance (Å)
1	Hydrophobic	LEU162	3.979
2	Hydrophobic	VAL196	3.665
3	Hydrophobic	ALA200	3.665
4	Hydrophobic	HIS203	3.753
5	Hydrogen bond	GLN167	3.338 (2.45 to H)
6	Hydrogen bond	SER208	2.708 (2.41 to H)

Section 5: Discussion

5.1 Overview of candidate selection strategy

Multiple Sclerosis (MS) remains a disease with limited therapeutic options, particularly in the progressive forms. Given the complex and heterogeneous nature of MS, drug repurposing presents a promising strategy to identify new treatments. In this study, two computational information paths from the DRIVE network were used to generate drug-target hypotheses: Path A (genes-proteins-drug) and Path B (genes-disease-drug) (**Figure 1**). Two drugs were selected: paclitaxel and isotretinoin.

Paclitaxel is a chemotherapeutic agent that binds β-tubulin, stabilizing microtubules and disrupting cell division (50). Isotretinoin, an oral retinoid used primarily to treat severe acne, is converted in-vivo to tretinoin, which binds to the retinoic acid receptors and CRABPI (47,51). The discussion below evaluates the final candidate targets identified from the DRIVE-based hypotheses, focusing on their interactions with paclitaxel and isotretinoin, and their potential therapeutic relevance in MS.

5.2 Evaluation of Path A-based candidate: Paclitaxel and NLRP3

In this section, the NLRP3-paclitaxel hypothesis will be discussed, beginning with its literature-based origin from the initial *BCL2* DRIVE output, followed by an assessment of the docking results, and concluding with a discussion of the potential treatment's relevance to MS.

5.2.1 BCL2: Initial Output from Path A

The only output of Path A for paclitaxel was *BCL2*, a gene which codes for BCL-2, an anti-apoptotic protein highly expressed in cancer cells to promote tumor cell survival and resistance (52). The direct binding of paclitaxel to BCL-2, an interaction relevant to the drug's anti-cancer effects, has been experimentally described through biosensor-based binding assays (53). The relevance of BCL-2 in MS has also been experimentally described: for instance, BCL-2 shows altered expression levels in oligodendrocytes of MS lesions; levels of phosphorylated BCL-2 are significantly decreased in non-responders to GA, and defective apoptotic deletion of autoreactive lymphocytes in MS patients contributes to CNS inflammation (54–56). Therefore, leveraging paclitaxel's ability to inhibit BCL-2 could help mitigate the formation of new lesions. That Path A identified a known, MS-relevant binding target of paclitaxel highlights its robustness and suggests its utility for uncovering novel MS targets.

5.2.2 Literature-based origin of NLRP3 as a paclitaxel target hypothesis

Based on Path A's *BCL2* output, a literature review was performed to identify an additional candidate target: *NLRP3*. Prior studies have confirmed the direct interaction between paclitaxel and BCL-2 protein, computationally characterizing the binding pocket, docking site, and key residues involved (53). Notably, parallels have been drawn between paclitaxel's binding to BCL-2 and β-tubulin, and the interactions of the orphan nuclear receptor Nur77 (a transcription factor whose endogenous ligand remains undefined) with these same proteins. This raises the possibility that paclitaxel may functionally mimic aspects of Nur77's activity (53).

In addition to BCL-2 and β-tubulin, NLRP3 has also been observed to interact directly with Nur77. Specifically, during pyroptosis induction, Nur77 translocates from the nucleus to the cytoplasm and colocalizes with NLRP3 in the trans-Golgi network, subsequently blocking NLRP3 oligomerization. This inhibition of NLRP3 complex formation prevents IL-1B release and downstream immune activation (57).

Therefore, building on: (1) Paclitaxel's known direct inhibition of BCL-2 and β-tubulin, (2) The parallel drawn between paclitaxel's binding and Nur77's interactions, and (3) The established direct Nur77-NLRP3 interaction, NLRP3 is a proposed potential novel target for paclitaxel. *NLRP3* was also present as a candidate in the unfiltered Path B hypotheses for paclitaxel, providing convergent evidence that supports NLRP3 as a possible target. The logical pathway connecting paclitaxel's known targets through Nur77 mimicry to inhibition of NLRP3 is summarized in **Figure 12.**

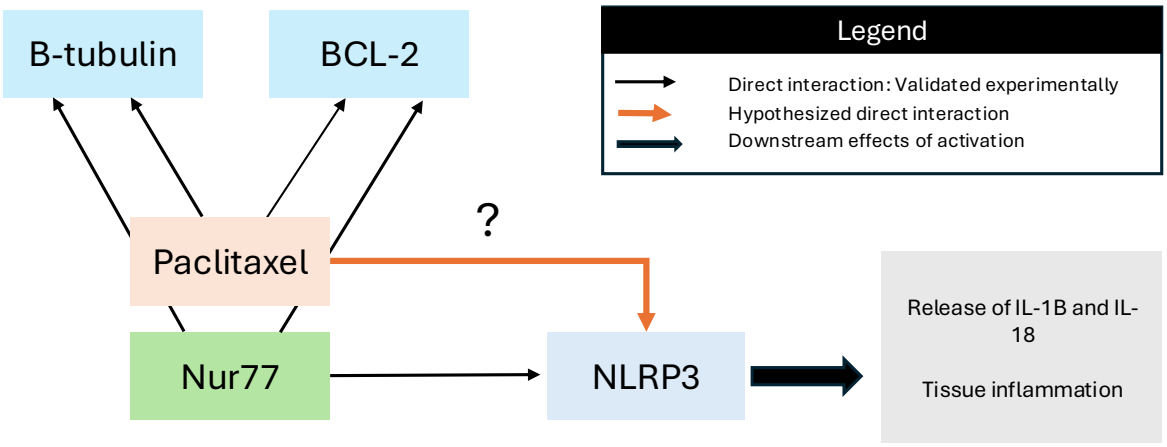

Figure 12. NLRP3 as a candidate target for paclitaxel treatment for MS

5.2.3 Docking validation: Paclitaxel and NLRP3

Docking was focused onto the NACHT domain of NLRP3 due to its physiological relevance. NLRP3 consists of three main domains: the PYD (pyrin domain), the central NACHT domain, and the C-terminal LRR (leucine-rich repeat) domain. The NACHT domain is essential for NLRP3 activation, as it mediates ATPase activity and oligomerization. Interaction with this region has shown to promote ubiquitination of NLRP3 and inhibitory effects (58). In contrast, interaction with the LRR domain has primed the activation of the inflammasome (59). Given the goal of inhibiting NLRP3 activation as a potential treatment strategy for multiple sclerosis, targeting the NACHT domain was particularly strategic.

The docking confirmed that paclitaxel binds to the NACHT domain of NLRP3 with a low Vina score (-9.9 kcal/mol), supporting its potential as a mechanistic target. The generated AF model resolved a critical missing loop in the cryo-EM structure, enabling more comprehensive pocket characterization (**Figure 6D**).

Several of the key interactions deemed essential in the paclitaxel-β-tubulin site were also observed in the paclitaxel-NLRP3 binding site. Hydrophobic interactions anchoring the C2, N', and C3' rings (60), the presence of prolines in the pocket (53), and hydrogen bonding with the 2'-OH group (61) were all maintained.

Notable differences between the two binding pockets included the nature and location of the π–π interactions. In the paclitaxel-β-tubulin site, they occurred between HIS229 and the C2 ring (**Figure 4B**), while in the paclitaxel-NLRP3 site, π–π interactions were between PHE275 and the N' phenyl ring (**Figure 6**). This discrepancy likely reflects differences in the binding

pocket architecture and the positioning of the aromatic residues, an expected outcome when comparing binding sites across structurally unrelated proteins.

Another key difference was the lack of close hydrogen bonding between the oxetane ring and surrounding residues in the NLRP3 pocket. The closest interaction was with SER658 at a distance of 4.927 Å, which is too far for even weak hydrogen bonding to occur .

The binding pocket of paclitaxel-NLRP3 also shared several key features with the Nur77 mimicry model proposed by (53), which suggests that paclitaxel mimics the endogenous ligand Nur77 when binding to BCL-2 and β-tubulin (pockets shown in **Figure 13).**

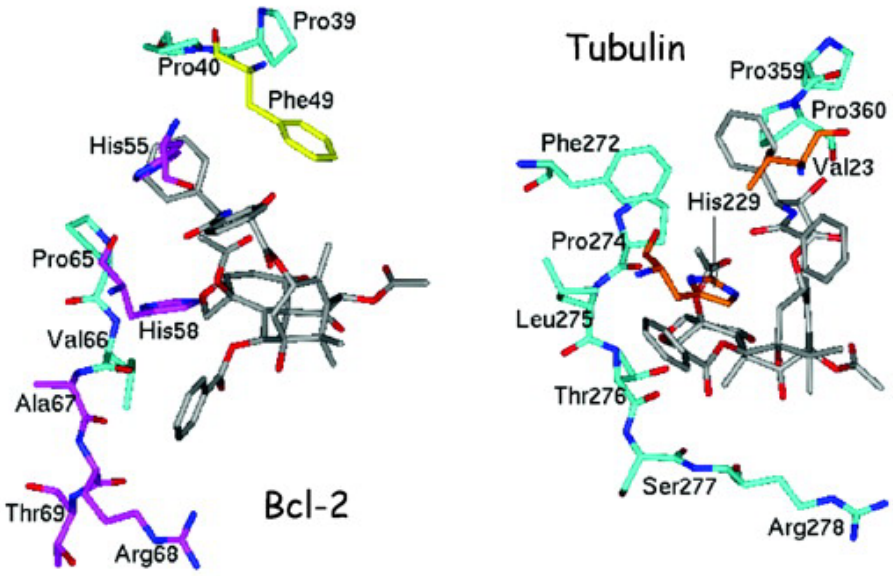

Figure 13. Modeled binding sites of paclitaxel in BCL-2 and in β-tubulin
Reprinted from (53), with permission from American Association of Cancer Research.

Like the conserved residues of PRO65-ARG68 in BCL-2 and PRO274-ARG278 in the β-tubulin, the paclitaxel-NLRP3 pocket had a structure that spans from PRO625 to ARG578. This structure interacted with the C2-phenyl and participated in hydrogen bonding with various side chain oxygens. Next, the PHE575 in NLRP3, which interacted with the N' phenyl, and PHE410, which interacted with the C3'-phenyl, resembles the PHE49 of BCL-2 and PHE272 of β-tubulin. Finally, ALA288 of NLRP3 formed similar hydrophobic bonds with the N'-phenyl ring as HIS55 (BCL-2) and VAL23 (β-tubulin). There are two discrepancies of the paclitaxel-NLRP3 pocket from the binding sites in **Figure 13**: a lack of adjacent proline residues (PRO39 and PRO40 in BCL-2 and PRO359 and PRO360 in β-tubulin) and a lack of close hydrophobic contacts with the oxetane ring. Despite these differences, the binding

pockets share several key characteristics, and nearly all essential interactions of paclitaxel were accounted for in the docked structure.

Another important inconsistency to consider regarding the docking of paclitaxel to NLRP3 is the difference in the paclitaxel conformers, as illustrated by **Figure 8**. The T-Taxol conformation, the form taken by β-tubulin-bound paclitaxel, is generally considered the mechanistically active form β-tubulin binding pocket (63). An alternative paclitaxel docking result on the AlphaFold-generated NLRP3 NACHT domain occupied the same region but adopted the T-shaped paclitaxel conformation (**Figure S3**). However, this conformer had a slightly higher VinaScore of -9.0 and was therefore not chosen for further analysis.

Paclitaxel is a relatively flexible molecule, except for its rigid taxane core. To date, its optimal binding conformation has primarily been characterized in complex with β-tubulin. However, docking alone cannot determine whether specific bond rotations impact paclitaxel's biological activity within other targets. Therefore, additional in-vitro experiments or molecular dynamics simulations are needed to determine the most active conformer of paclitaxel when bound to NLRP3.

5.2.4 Therapeutic potential and dual effects of targeting NLRP3 with paclitaxel in MS

Whether inhibition of NLRP3 is a plausible treatment method for MS, and whether paclitaxel is an ideal candidate for this purpose, requires further discussion. The NLRP3 protein, the sensor component of the NLRP3 inflammasome, plays a central role in detecting Damage-Associated Molecular Patterns (DAMPs) and Pathogen-Associated Molecular Patterns (PAMPs) and mediating inflammatory responses (64). In MS, the NLRP3 inflammasome contributes to the development of experimental autoimmune encephalomyelitis (EAE), the animal model of MS, by aiding the migration of T-helper cells to the CNS and inducing pro-inflammatory cytokine release (65,66).

Although most research about MS focuses on T-cells as the key player of MS pathogenesis, recent studies highlight the role of B-cells in the disease through the production of cytokines and interaction with T cells (67). B-cell-activating factors may also stimulate the NLRP3 inflammasome, but this mechanism remains to be further explored. Finally, the NLRP3 protein is elevated in the monocytes of MS patients compared to healthy individuals (68). Given its pro-inflammatory role, targeting NLRP3 activity may help mitigate the autoimmune response in MS.

Assuming paclitaxel engages NLRP3 in a manner that mimics Nur77, as has been proposed for its interactions with BCL-2 and β-tubulin (**Figure 12)**, it is important to consider the context-dependent nature of the Nur77-NLRP3 interaction. While Nur77 has been shown to sequester NLRP3 to the trans-Golgi and block inflammasome assembly (57), it has also been reported to promote NLRP3 activation through direct binding to cytoplasmic lipopolysaccharide in the presence of double-stranded DNA (dsDNA) (69). Despite this potential activating role, other studies, particularly in models of colitis and endotoxin-induced inflammation, show that Nur77 deficiency leads to heightened NLRP3 activation and increased inflammatory responses (70). This suggests that Nur77 acts as a context-dependent modulator, but mimicking its inhibitory interaction with NLRP3 may be a compelling method of restraining the inflammasome in the context of MS.

Docking results indicate a plausible direct interaction between paclitaxel and the NACHT domain of NLRP3, supporting its potential role as an inhibitor and therapeutic candidate for MS. However, paclitaxel has also been shown to indirectly activate NLRP3 in some contexts, through its microtubule stabilization (71). These seemingly conflicting effects may depend on factors like dosage, cell type, and timing, and highlight the importance of understanding context when repurposing paclitaxel. Within the CNS, paclitaxel has demonstrated both neurotoxic and neuroprotective effects: while it promotes axonal regeneration and reduces glial scar formation in animal models of nerve injury (72), it also increases the risk of peripheral neuropathy and impaired neural function (73). In short, β-tubulin-targeting drugs can exert both beneficial and adverse effects in the CNS.

Still, dual inhibition of BCL-2 and NLRP3 by paclitaxel could offer meaningful therapeutic benefits for MS, especially if its direct interaction with NLRP3 is inhibitory in relevant cell types. Although its effects in human patients remain uncharacterized, paclitaxel has been shown to delay the onset of CNS disease in the mouse model of MS, further supporting its potential as a treatment candidate (74).

5.3 Path B: MMP1 as a Potential Novel Target for Paclitaxel and Tretinoin

5.3.1 Rationale for MMP1 Selection

From the initial Path B candidate lists, *MMP1* was selected as a target candidate for both paclitaxel and tretinoin as it did not have the immune system processes GO term, it had fewer than five PPI connections, and had a 3D structure available on PDB. Matrix metalloproteinases (MMPs) play an important role in the immunopathogenesis of MS by disrupting the BBB,

recruiting inflammatory cells into the CNS, and enhancing the demyelination process (75). MMP1 is a collagenase that belongs to this family of proteins and is an activator for MMP2 and MMP9, both proteins which increase the permeability of the BBB. Additionally, there is an increased expression of MMP1 in cerebrospinal fluid and brain tissue of MS patients (76,77). Inhibiting MMP1 could thus provide an effective method of preventing the disruption of BBB, mitigating migration of non-native immune cells to the CNS, and ultimately decreasing inflammation and MS pathogenesis.

5.3.2 Docking validation analysis of Paclitaxel with MMP1

To validate whether the paclitaxel-MMP1 complex was a plausible drug-target hypothesis in the context of MS treatment through docking, the binding site on MMP1 was considered in addition to the similarity of the binding pocket to the reference. Inhibitors of MMP1 bind to the protein's active site, which is located within the catalytic domain and characterized by a zinc ion coordinated by three histidine residues and a water molecule. The catalytic zinc ion is bound by HIS199, HIS203, and HIS209, and MMP1 inhibitors typically coordinate directly with the zinc ion through a zinc binding group (78,79).

Although paclitaxel docked to MMP1 in the active site had the second-best Vina score, it was selected for further analysis and comparison with the reference binding site due to its biological relevance. There were several interactions with binding pocket residues that matched the reference binding pocket, such as hydrophobic interactions with the N' phenyl ring and hydrogen bonding of the oxetane ring (**Figure 9B, Table 6**). However, several interactions that are essential for paclitaxel activity were missing in this binding pocket. For example, there was no hydrophobic interactions stabilizing neither the C3' nor the C2 phenyl rings. In addition, while there were several aromatic residues present (**Figure 9A)** there was only one aromatic residue (TYR221) that had proximity to a phenyl ring, indicating that π–π bonds with the phenyl rings of paclitaxel would be unlikely. In terms of the binding conformer of paclitaxel, it exhibited a T-Taxol form like that of the reference, with a few minor rotations of carbons, which are annotated in **Figure 10**. As mentioned, one significant characteristic of an MMP inhibitor is coordination with the zinc ion. In the predicted binding conformer, the closest interacting group with zinc was the C2' hydroxyl, which in β-tubulin forms a hydrogen bond with PRO360. This oxygen is 1.391 Å away from the zinc ion, so its coordination with zinc is possible but likely weak, given that hydroxyls are not among the frequently found zinc binding groups of ligands (80).

Despite the similarity of the structural binding conformer and the possible coordination with the zinc ion, the missing key residue interactions and the small, shallow binding pocket suggest that paclitaxel is likely not an ideal binding candidate of MMP1.

5.3.3 Docking validation analysis of Tretinoin with MMP1

Tretinoin bound to the active site of MMP1 also had the second highest Vina score of -6.9. As with the binding site with that of CRABP1, there were several hydrophobic residues interacting with the hydrocarbon chain of tretinoin. There were also hydrogen bonds of the carboxylic acid group oxygen atoms interacting with GLN167 and SER208, further stabilizing the ligand in the pocket.

Despite these interactions, tretinoin is not likely to bind into this pocket of MMP1 for several reasons. Firstly, there is no salt bridge of the carboxylate oxygens with ARG, an interaction that is essential for tretinoin activity, not just in the modeled reference CRABPI but also in other retinoic acid receptors, such as RARα, RARβ, and RARγ (81,82). Secondly, there are no zinc binding groups in proximity to the zinc ion, meaning that inhibitory action within MMP1 is unlikely.

Section 6: Conclusions and Future Directions

This thesis aimed to identify and evaluate potential drug-target interactions relevant to multiple sclerosis (MS), using DRIVE-based repurposing hypotheses, a custom filtering pipeline, and molecular modeling techniques. While the process yielded mixed outcomes, it highlights the promise and limitations of computational drug repurposing strategies in the context of MS and establishes a foundational framework for integrating network medicine-based repurposing hypotheses with structural computational data. The key findings were as follows:

1. A filtering pipeline was developed to prioritize novel drug-target candidates.
2. Application of the pipeline to candidate targets of paclitaxel and isotretinoin yielded MMP1 as a potential target. However, docking results did not support a viable drug-target interaction.
3. A gene-protein-drug-based approach identified NLRP3 as a promising target for paclitaxel, supported by favorable docking results.

This work also had important limitations. Docking studies, while useful for an initial screening, lack precision and thus cannot be considered definitive evidence of binding. In particular, CB-Dock2, the tool used in this thesis, performs rigid receptor docking and cannot account for protein flexibility, which can impact docking results. Furthermore, the potential impact of genetic variants in MS patients, such as polymorphisms in *NLRP3* or *MMP1*, was not addressed and could affect the relevance of the proposed hypotheses.

Future work should focus on validating the paclitaxel-NLRP3 interaction through molecular dynamics simulations to assess binding stability and conformational dynamics. In parallel, other target candidates in the final candidate lists from the DRIVE predictions could be further explored. To improve the docking studies, tools that support flexible side-chain docking could be employed, which may better simulate interactions between drugs and proteins with dynamic binding pockets. Ultimately, experimental validation in MS-relevant models is necessary to determine the therapeutic potential of the predicted interactions.

References

1. Walton C, King R, Rechtman L, Kaye W, Leray E, Marrie RA, et al. Rising prevalence of multiple sclerosis worldwide: Insights from the Atlas of MS, third edition. Mult Scler J. 2020 Dec;26(14):1816–21.

2. Dutta R, Trapp BD. Relapsing and progressive forms of multiple sclerosis: insights from pathology. Curr Opin Neurol. 2014 Jun;27(3):271–8.

3. Dighriri IM, Aldalbahi AA, Albeladi F, Tahiri AA, Kinani EM, Almohsen RA, et al. An Overview of the History, Pathophysiology, and Pharmacological Interventions of Multiple Sclerosis. Cureus [Internet]. 2023 Jan 2 [cited 2025 Jun 24]; Available from: https://www.cureus.com/articles/131339-an-overview-of-the-history-pathophysiology-and-pharmacological-interventions-of-multiple-sclerosis

4. Sriram S. Role of glial cells in innate immunity and their role in CNS demyelination. J Neuroimmunol. 2011 Oct;239(1–2):13–20.

5. Alfredsson L, Olsson T. Lifestyle and Environmental Factors in Multiple Sclerosis. Cold Spring Harb Perspect Med. 2019 Apr;9(4):a028944.

6. Hauser SL, Cree BAC. Treatment of Multiple Sclerosis: A Review. Am J Med. 2020 Dec;133(12):1380-1390.e2.

7. Saleem S, Anwar A, Fayyaz M, Anwer F, Anwar F. An Overview of Therapeutic Options in Relapsing-remitting Multiple Sclerosis. Cureus [Internet]. 2019 Jul 26 [cited 2025 May 28]; Available from: https://www.cureus.com/articles/21600-an-overview-of-therapeutic-options-in-relapsing-remitting-multiple-sclerosis

8. Dhib-Jalbut S, Marks S. Interferon-β mechanisms of action in multiple sclerosis. Neurology [Internet]. 2010 Jan 5 [cited 2025 May 28];74(1_supplement_1). Available from: https://www.neurology.org/doi/10.1212/WNL.0b013e3181c97d99

9. Aharoni R. Immunomodulation neuroprotection and remyelination – The fundamental therapeutic effects of glatiramer acetate: A critical review. J Autoimmun. 2014 Nov;54:81–92.

10. Chisari CG, Bianco A, Brescia Morra V, Calabrese M, Capone F, Cavalla P, et al. Effectiveness of Ocrelizumab in Primary Progressive Multiple Sclerosis: a Multicenter, Retrospective, Real-world Study (OPPORTUNITY). Neurotherapeutics. 2023 Oct;20(6):1696–706.

11. Bano I, Butt UD, Mohsan SAH. New challenges in drug discovery. In: Novel Platforms for Drug Delivery Applications [Internet]. Elsevier; 2023 [cited 2025 May 29]. p. 619–43. Available from: https://linkinghub.elsevier.com/retrieve/pii/B9780323913768000215

12. Pushpakom S, Iorio F, Eyers PA, Escott KJ, Hopper S, Wells A, et al. Drug repurposing: progress, challenges and recommendations. Nat Rev Drug Discov. 2019 Jan;18(1):41–58.

13. Trejo-Castro AI, Martinez-Ledesma E, Martinez-Torteya A. A bibliometric review on in silico drug repurposing: Performance analysis, science mapping and text mining (2000–2023). Heliyon. 2025 May;11(10):e42750.

14. Agu PC, Afiukwa CA, Orji OU, Ezeh EM, Ofoke IH, Ogbu CO, et al. Molecular docking as a tool for the discovery of molecular targets of nutraceuticals in diseases management. Sci Rep. 2023 Aug 17;13(1):13398.

15. Szklarczyk D, Kirsch R, Koutrouli M, Nastou K, Mehryary F, Hachilif R, et al. The STRING database in 2023: protein–protein association networks and functional enrichment analyses for any sequenced genome of interest. Nucleic Acids Res. 2023 Jan 6;51(D1):D638–46.

16. Prieto Santamaría L, Díaz Uzquiano M, Ugarte Carro E, Ortiz-Roldán N, Pérez Gallardo Y, Rodríguez-González A. Integrating heterogeneous data to facilitate COVID-19 drug repurposing. Drug Discov Today. 2022 Feb;27(2):558–66.

17. Durrant JD, McCammon JA. Molecular dynamics simulations and drug discovery. BMC Biol. 2011 Dec;9(1):71.

18. Subramanian A, Narayan R, Corsello SM, Peck DD, Natoli TE, Lu X, et al. A Next Generation Connectivity Map: L1000 Platform and the First 1,000,000 Profiles. Cell. 2017 Nov;171(6):1437-1452.e17.

19. Qiao H, Chen Y, Qian C, Guo Y. Clinical data mining: challenges, opportunities, and recommendations for translational applications. J Transl Med. 2024 Feb 20;22(1):185.

20. Le BL, Andreoletti G, Oskotsky T, Vallejo-Gracia A, Rosales R, Yu K, et al. Transcriptomics-based drug repositioning pipeline identifies therapeutic candidates for COVID-19. Sci Rep. 2021 Jun 10;11(1):12310.

21. Bojkova D, Klann K, Koch B, Widera M, Krause D, Ciesek S, et al. Proteomics of SARS-CoV-2-infected host cells reveals therapy targets. Nature. 2020 Jul 16;583(7816):469–72.

22. Cheng F, Lu W, Liu C, Fang J, Hou Y, Handy DE, et al. A genome-wide positioning systems network algorithm for in silico drug repurposing. Nat Commun. 2019 Aug 2;10(1):3476.

23. Goh KI, Cusick ME, Valle D, Childs B, Vidal M, Barabási AL. The human disease network. Proc Natl Acad Sci. 2007 May 22;104(21):8685–90.

24. Zhou X, Menche J, Barabási AL, Sharma A. Human symptoms–disease network. Nat Commun. 2014 Jun 26;5(1):4212.

25. Piñero J, Ramírez-Anguita JM, Saüch-Pitarch J, Ronzano F, Centeno E, Sanz F, et al. The DisGeNET knowledge platform for disease genomics: 2019 update. Nucleic Acids Res. 2019 Nov 4;gkz1021.

26. Marinho EM, Batista De Andrade Neto J, Silva J, Rocha Da Silva C, Cavalcanti BC, Marinho ES, et al. Virtual screening based on molecular docking of possible inhibitors of Covid-19 main protease. Microb Pathog. 2020 Nov;148:104365.

27. Singh S, Bajpai U, Lynn AM. Structure based virtual screening to identify inhibitors against MurE Enzyme of Mycobacterium tuberculosis using AutoDock Vina. Bioinformation. 2014;10(11):697–702.

28. Abramson J, Adler J, Dunger J, Evans R, Green T, Pritzel A, et al. Accurate structure prediction of biomolecular interactions with AlphaFold 3. Nature. 2024 Jun 13;630(8016):493–500.

29. Scardino V, Di Filippo JI, Cavasotto CN. How good are AlphaFold models for docking-based virtual screening? iScience. 2023 Jan;26(1):105920.

30. Gaillard T. Evaluation of AutoDock and AutoDock Vina on the CASF-2013 Benchmark. J Chem Inf Model. 2018 Aug 27;58(8):1697–706.

31. Verdonk ML, Cole JC, Hartshorn MJ, Murray CW, Taylor RD. Improved protein–ligand docking using GOLD. Proteins Struct Funct Bioinforma. 2003 Sep;52(4):609–23.

32. Friesner RA, Banks JL, Murphy RB, Halgren TA, Klicic JJ, Mainz DT, et al. Glide: A New Approach for Rapid, Accurate Docking and Scoring. 1. Method and Assessment of Docking Accuracy. J Med Chem. 2004 Mar 1;47(7):1739–49.

33. Vreven T, Hwang H, Pierce BG, Weng Z. Evaluating template-based and template-free protein-protein complex structure prediction. Brief Bioinform. 2014 Mar 1;15(2):169–76.

34. Kundrotas PJ, Lensink MF, Alexov E. Homology-based modeling of 3D structures of protein–protein complexes using alignments of modified sequence profiles. Int J Biol Macromol. 2008 Aug;43(2):198–208.

35. Mukherjee S, Zhang Y. Protein-Protein Complex Structure Predictions by Multimeric Threading and Template Recombination. Structure. 2011 Jul;19(7):955–66.

36. Sinha R, Kundrotas PJ, Vakser IA. Docking by structural similarity at protein-protein interfaces. Proteins Struct Funct Bioinforma. 2010 Nov 15;78(15):3235–41.

37. Liu Y, Yang X, Gan J, Chen S, Xiao ZX, Cao Y. CB-Dock2: improved protein–ligand blind docking by integrating cavity detection, docking and homologous template fitting. Nucleic Acids Res. 2022 Jul 5;50(W1):W159–64.

38. Wu Q, Peng Z, Zhang Y, Yang J. COACH-D: improved protein–ligand binding sites prediction with refined ligand-binding poses through molecular docking. Nucleic Acids Res. 2018 Jul 2;46(W1):W438–42.

39. Ayuso-Muñoz A, Prieto-Santamaría L, Ugarte-Carro E, Serrano E, Rodríguez-González A. Uncovering hidden therapeutic indications through drug repurposing with graph neural networks and heterogeneous data. Artif Intell Med. 2023 Nov;145:102687.

40. Raudvere U, Kolberg L, Kuzmin I, Arak T, Adler P, Peterson H, et al. g:Profiler: a web server for functional enrichment analysis and conversions of gene lists (2019 update). Nucleic Acids Res. 2019 Jul 2;47(W1):W191–8.

41. Dendrou CA, Fugger L, Friese MA. Immunopathology of multiple sclerosis. Nat Rev Immunol. 2015 Sep;15(9):545–58.

42. Bairoch A, Lane L. neXtProt Data release 2023-09-11 [Internet]. Zenodo; 2023 [cited 2025 Jun 1]. Available from: https://zenodo.org/doi/10.5281/zenodo.14163587

43. Jeong H, Mason SP, Barabási AL, Oltvai ZN. Lethality and centrality in protein networks. Nature. 2001 May;411(6833):41–2.

44. Zotenko E, Mestre J, O'Leary DP, Przytycka TM. Why Do Hubs in the Yeast Protein Interaction Network Tend To Be Essential: Reexamining the Connection between the Network Topology and Essentiality. Rost B, editor. PLoS Comput Biol. 2008 Aug 1;4(8):e1000140.

45. Han JDJ, Bertin N, Hao T, Goldberg DS, Berriz GF, Zhang LV, et al. Evidence for dynamically organized modularity in the yeast protein–protein interaction network. Nature. 2004 Jul 1;430(6995):88–93.

46. Tejera-Nevado P, Junod N, Kwon EH, Prieto-Santamaría L, Rodríguez-González A. Benchmarking Docking Tools on Experimental and Artificial Intelligence-Predicted Protein Structures [Internet]. 2025 [cited 2025 Jul 2]. Available from: http://biorxiv.org/lookup/doi/10.1101/2025.06.03.657620

47. Layton A. The use of isotretinoin in acne. Dermatoendocrinol. 2009 May;1(3):162–9.

48. Ghersi D, Sanchez R. Improving accuracy and efficiency of blind protein-ligand docking by focusing on predicted binding sites. Proteins Struct Funct Bioinforma. 2009 Feb;74(2):417–24.

49. Adasme MF, Linnemann KL, Bolz SN, Kaiser F, Salentin S, Haupt VJ, et al. PLIP 2021: expanding the scope of the protein–ligand interaction profiler to DNA and RNA. Nucleic Acids Res. 2021 Jul 2;49(W1):W530–4.

50. Cheung CHA, Chen HH, Kuo CC, Chang CY, Coumar MS, Hsieh HP, et al. Survivin counteracts the therapeutic effect of microtubule de-stabilizers by stabilizing tubulin polymers. Mol Cancer. 2009 Dec;8(1):43.

51. Yadav AS, Stevison F, Kosaka M, Wong S, Kenny JR, Amory JK, et al. Isotretinoin and its Metabolites Alter mRNA of Multiple Enzyme and Transporter Genes In Vitro, but Downregulation of Organic Anion Transporting Polypeptide Does Not Translate to the Clinic. Drug Metab Dispos. 2022 Jul;50(7):1042–52.

52. Youle RJ, Strasser A. The BCL-2 protein family: opposing activities that mediate cell death. Nat Rev Mol Cell Biol. 2008 Jan;9(1):47–59.

53. Ferlini C, Cicchillitti L, Raspaglio G, Bartollino S, Cimitan S, Bertucci C, et al. Paclitaxel Directly Binds to Bcl-2 and Functionally Mimics Activity of Nur77. Cancer Res. 2009 Sep 1;69(17):6906–14.

54. Anselmo F, Tatomir A, Boodhoo D, Mekala AP, Nguyen V, Rus V, et al. JNK and phosphorylated Bcl-2 predict multiple sclerosis clinical activity and glatiramer acetate therapeutic response. Clin Immunol. 2020 Jan;210:108297.

55. Correale J, Gilmore W, Li S, Walsh J, Bassani MM, Lund B, et al. Resistance to glucocorticoid-induced apoptosis in PLP peptide-specific T cell clones from patients with progressive MS. J Neuroimmunol. 2000 Sep;109(2):197–210.

56. Sharief MK, Matthews H, Noori MA. Expression ratios of the Bcl-2 family proteins and disease activity in multiple sclerosis. J Neuroimmunol. 2003 Jan;134(1–2):158–65.

57. Deng Z, Yang Z, Cui C, Wei H, Wang L, Tian D, et al. NR4A1 suppresses pyroptosis by transcriptionally inhibiting NLRP3 and IL-1β and co-localizing with NLRP3 in trans-Golgi to alleviate pathogenic bacteria-induced colitis. Clin Transl Med. 2021 Dec;11(12):e639.

58. Tang T, Li P, Zhou X, Wang R, Fan X, Yang M, et al. The E3 Ubiquitin Ligase TRIM65 Negatively Regulates Inflammasome Activation Through Promoting Ubiquitination of NLRP3. Front Immunol. 2021 Aug 26;12:741839.

59. Zhu K, Jin X, Chi Z, Chen S, Wu S, Sloan RD, et al. Priming of NLRP3 inflammasome activation by Msn kinase MINK1 in macrophages. Cell Mol Immunol. 2021 Oct;18(10):2372–82.

60. Löwe J, Li H, Downing KH, Nogales E. Refined structure of αβ-tubulin at 3.5 Å resolution 1 1Edited by I. A. Wilson. J Mol Biol. 2001 Nov;313(5):1045–57.

61. Sharma S, Lagisetti C, Poliks B, Coates RM, Kingston DGI, Bane S. Dissecting Paclitaxel–Microtubule Association: Quantitative Assessment of the 2′-OH Group. Biochemistry. 2013 Apr 2;52(13):2328–36.

62. MacLeod JM, Rosei F. Directed Assembly of Nanostructures. In: Comprehensive Nanoscience and Technology [Internet]. Elsevier; 2011 [cited 2025 Jul 4]. p. 13–68. Available from: https://linkinghub.elsevier.com/retrieve/pii/B9780123743961000982

63. Bozdaganyan M, Fedorov V, Kholina E, Kovalenko I, Gudimchuk N, Orekhov P. Exploring tubulin-paclitaxel binding modes through extensive molecular dynamics simulations. Sci Rep. 2025 Mar 11;15(1):8378.

64. Peñin-Franch A, García-Vidal JA, Martínez CM, Escolar-Reina P, Martínez-Ojeda RM, Gómez AI, et al. Galvanic current activates the NLRP3 inflammasome to promote Type I collagen production in tendon. eLife. 2022 Feb 24;11:e73675.

65. Inoue M, Williams KL, Gunn MD, Shinohara ML. NLRP3 inflammasome induces chemotactic immune cell migration to the CNS in experimental autoimmune encephalomyelitis. Proc Natl Acad Sci. 2012 Jun 26;109(26):10480–5.

66. Olcum M, Tastan B, Kiser C, Genc S, Genc K. Microglial NLRP3 inflammasome activation in multiple sclerosis. In: Advances in Protein Chemistry and Structural Biology [Internet]. Elsevier; 2020 [cited 2025 Jun 22]. p. 247–308. Available from: https://linkinghub.elsevier.com/retrieve/pii/S1876162319300616

67. Lazibat I. Multiple Sclerosis: New Aspects of Immunopathogenesis. Acta Clin Croat [Internet]. 2018 [cited 2025 Jun 22];57(2). Available from: https://hrcak.srce.hr/index.php?show=clanak&id_clanak_jezik=304956

68. Cui Y, Yu H, Bu Z, Wen L, Yan L, Feng J. Focus on the Role of the NLRP3 Inflammasome in Multiple Sclerosis: Pathogenesis, Diagnosis, and Therapeutics. Front Mol Neurosci. 2022 May 25;15:894298.

69. Zhu F, Ma J, Li W, Liu Q, Qin X, Qian Y, et al. The orphan receptor Nur77 binds cytoplasmic LPS to activate the non-canonical NLRP3 inflammasome. Immunity. 2023 Apr;56(4):753-767.e8.

70. Yuan R, Zhang W, Nie P, Lan K, Yang X, Yin A, et al. Nur77 Deficiency Exacerbates Macrophage NLRP3 Inflammasome-Mediated Inflammation and Accelerates Atherosclerosis. Zhou Y, editor. Oxid Med Cell Longev. 2022 Jan;2022(1):2017815.

71. Liu Y, Guo Z wei, Li J, Li A hong, Huo T guang. Insight into the regulation of NLRP3 inflammasome activation by mitochondria in liver injury and the protective role of natural products. Biomed Pharmacother. 2022 Dec;156:113968.

72. Hellal F, Hurtado A, Ruschel J, Flynn KC, Laskowski CJ, Umlauf M, et al. Microtubule Stabilization Reduces Scarring and Causes Axon Regeneration After Spinal Cord Injury. Science. 2011 Feb 18;331(6019):928–31.

73. Wolf S, Barton D, Kottschade L, Grothey A, Loprinzi C. Chemotherapy-induced peripheral neuropathy: Prevention and treatment strategies. Eur J Cancer. 2008 Jul;44(11):1507–15.

74. Crume KP, O'Sullivan D, Miller JH, Northcote PT, La Flamme AC. Delaying the onset of experimental autoimmune encephalomyelitis with the microtubule-stabilizing compounds, paclitaxel and Peloruside A. J Leukoc Biol. 2009 Aug 4;86(4):949–58.

75. Mirshafiey A, Asghari B, Ghalamfarsa G, Niaragh FJ, Azizi G. The Significance of Matrix Metalloproteinases in the Immunopathogenesis and Treatment of Multiple Sclerosis = أهمية الأنزيمات المعدنية المحللة للبروتين في تطور مرض التصلب العصبي المتعدد و علاجه. Sultan Qaboos Univ Med J. 2014 Feb;14(1):13–25.

76. Gijbels K, Masure S, Carton H, Opdenakker G. Gelatinase in the cerebrospinal fluid of patients with multiple sclerosis and other inflammatory neurological disorders. J Neuroimmunol. 1992 Nov;41(1):29–34.

77. Kouwenhoven M, Özenci V, Gomes A, Yarilin D, Giedraitis V, Press R, et al. Multiple sclerosis: elevated expression of matrix metalloproteinases in blood monocytes. J Autoimmun. 2001 Jun;16(4):463–70.

78. Almutairi S, Kalloush HM, Manoon NA, Bardaweel SK. Matrix Metalloproteinases Inhibitors in Cancer Treatment: An Updated Review (2013–2023). Molecules. 2023 Jul 21;28(14):5567.

79. Iyer S, Visse R, Nagase H, Acharya KR. Crystal Structure of an Active Form of Human MMP-1. J Mol Biol. 2006 Sep;362(1):78–88.

80. Kawai K, Nagata N. Metal–ligand interactions: An analysis of zinc binding groups using the Protein Data Bank. Eur J Med Chem. 2012 May;51:271–6.

81. Zhang ZP, Hutcheson JM, Poynton HC, Gabriel JL, Soprano KJ, Soprano DR. Arginine of retinoic acid receptor β which coordinates with the carboxyl group of retinoic acid functions independent of the amino acid residues responsible for retinoic acid receptor subtype ligand specificity. Arch Biochem Biophys. 2003 Jan;409(2):375–84.

82. Kleywegt GJ, Bergfors T, Senn H, Motte PL, Gsell B, Shud K, et al. Crystal structures of cellular retinoic acid binding proteins I and II in complex with all-trans-retinoic acid and a synthetic retinoid. Structure. 1994 Dec;2(12):1241–58.

83. Yu H, Li D, Xu F, Pan Q, Chai P, Liu B, et al. The binding affinity of human serum albumin and paclitaxel through MMPBSA based on docked complex. Mol Simul. 2016 Nov 21;42(17):1460–7.

Supplementary Materials

Table S1. DRIVE drug outputs

Drug ID	Drug Name	Paths with output	Redirection score
CHEMBL1023	Bexarotene	B	0
CHEMBL408	Troglitazone	A, B	0.0000000340714
CHEMBL428647	Paclitaxel	A, B	1
CHEMBL547	Isotretinoin	B	0
CHEMBL553	Erlotinib	B	0
CHEMBL92	Docetaxel	B	0

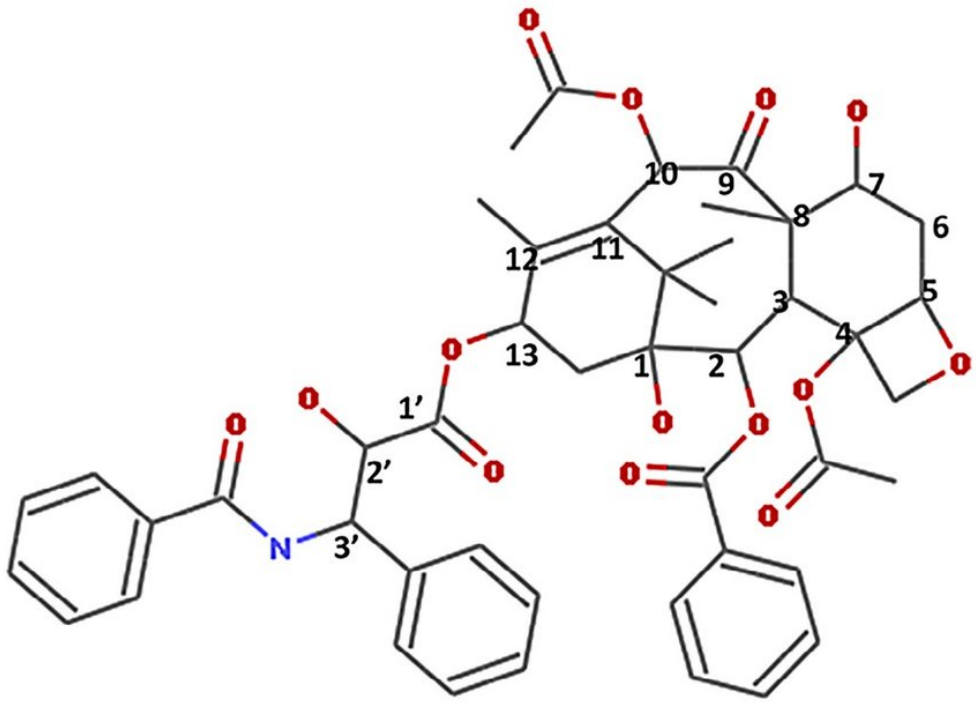

Figure S1. Labeled paclitaxel 2D structure
Figure reprinted from (83).

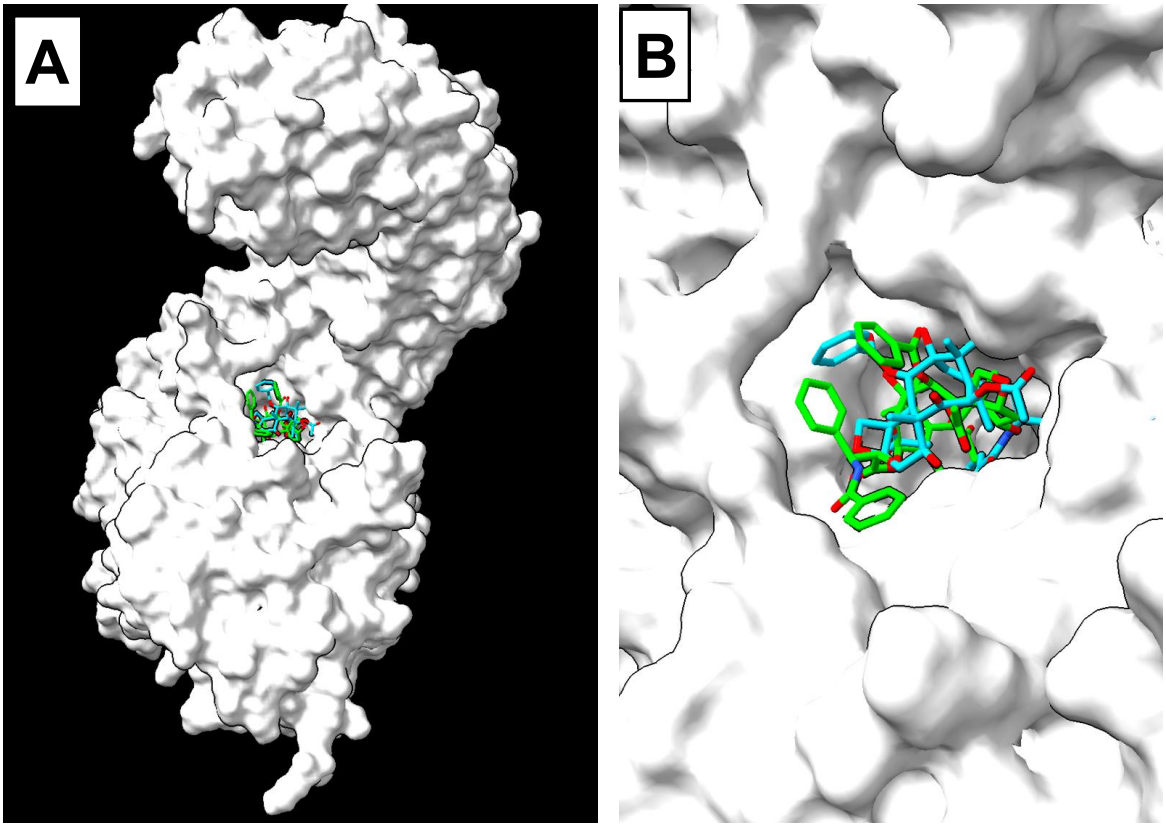

Figure S2. Identified binding pocket for NLRP3 NACHT vs. NLRP3 full structure
Best docking results from CB-Dock2 for FULL protein 9MGY and protein cut for just the NACHT domain. Green is conformer for query with all domains; Cyan is just when docked with NACHT.

Table S2. Alphafold-NLRP3 model analysis

Model #	Sequence Alignment Score	RMSD (Å) of pruned atoms	pLDDT
0	4359.6	0.919	77.40
1	4376.6	0.893	77.51
2	4369.4	0.980	77.58
3	4344.8	1.016	77.68
4	4370.6	1.014	77.71

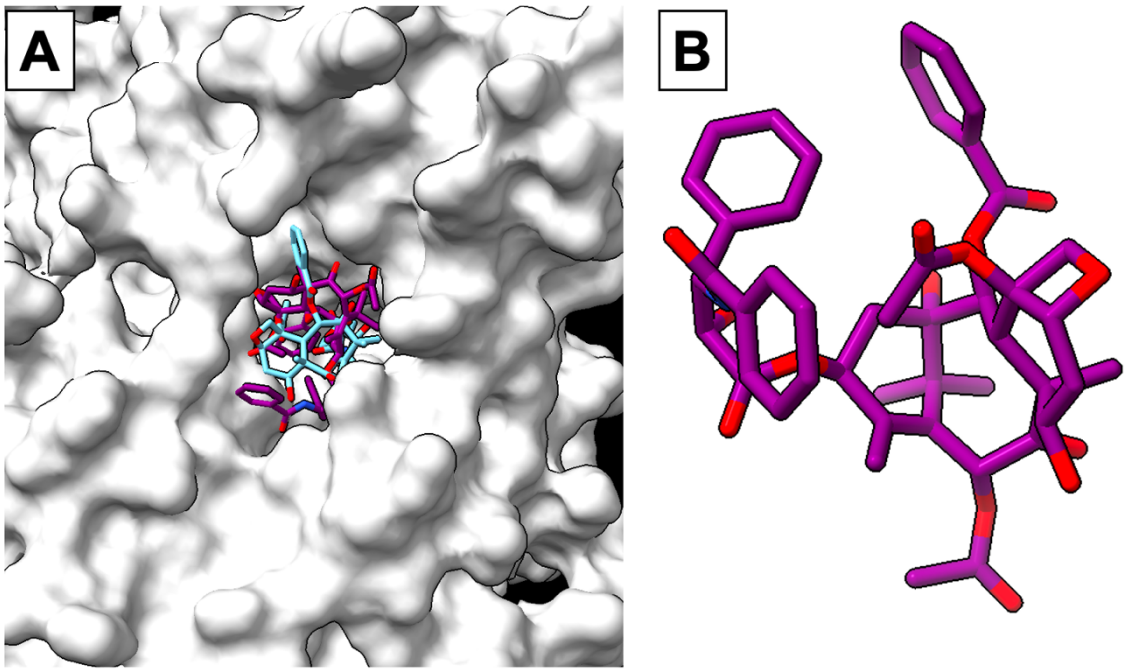

Figure S3. AF-NLRP3 NACHT with paclitaxel domain: pocket 2
The binding pocket of the second-place docking (in terms of vina score) is shown for AF_NLRP3 NACHT domain query with paclitaxel. It had a T-Taxol conformer, a vina score of -9.0, a cavity volume of 3773 $Å^3$ and the following pocket residues: GLU176 GLN180 ARG183 GLN225 GLY226 ALA227 ALA228 PRO352 VAL353 LEU355 GLU356 GLU369 PHE568 ILE574 PHE575 ARG578 SER626 LEU628 GLU629 TYR632 ASN656 SER658 THR659 ASP662.

Table S3. Final isotretinoin hypotheses from Path B

Gene symbol	UniProt ID
NOTCH4	Q99466
INS IGF2	F8WCM5
ERVW-1	Q9UQF0
SLC2A4RG	Q9NR83
CYP2R1	Q6VVX0
MMP1	P03956
CYP2D6	P10635
PTHLH	P12272
KCNH7	Q9NS40
SEC14L2	O76054
ERVK-11	Q9UQG0

Table S4. Final paclitaxel hypotheses from Path B

Gene symbol	UniProt ID
NOTCH4	Q99466
PPT2	Q9UMR5
ERVW-1	Q9UQF0
SLC2A4RG	Q9NR83
CYP2R1	Q6VVX0
MMP1	P03956
PTHLH	P12272
CYP2D6	P10635
SEC14L2	O76054
ERVK-11	Q9UQG0

Table S5. Top two best binding pockets from MMP1-Tretinoin docking

Target-Ligand	Pocket Number	Cavity Volume (Å³)	Vina Score (kcal/mol)	Predicted Pocket Residues
MMP1-Tretinoin	1	367	-7.5	PHE188 TYR221 THR222 PHE223 SER224 PHE297 SER299 VAL300 PRO303 GLN304 ASN336
	2	228	-6.9	THR84 GLU85 ASN161 LEU162 ALA163 HIS164 ALA165 PHE166 GLN167 VAL196 HIS199 ALA200 HIS203 LEU207 SER208 HIS209 PRO219 SER220

Table S6. Top two best binding pockets for MMP1-Paclitaxel docking

Target-Ligand	Pocket Number	Cavity Volume (Å³)	Vina Score (kcal/mol)	Predicted Pocket Residues
MMP1-Paclitaxel	1	420	-8.2	THR269 THR270 ARG272 GLY273 ASN287 PHE289 TYR313 GLU314 PHE315 ALA316 ASP317 ALA361 LEU362 SER363 GLU364 GLU365 ASN366 GLU383 TYR384 VAL410 PHE411 MET412 LYS413 ASP414
	2	228	-8.0	THR84 SER153 ASN161 LEU162 ALA163 HIS164 ALA165 PHE166 GLN167 HIS199 HIS203 LEU207 SER208 HIS209 PRO219 SER220 TYR221